Supporting Information

Molecular Rotational Conformation Controls the Rate of Singlet Fission and Triplet Decay in Pentacene Dimers

Rasmus Ringström,[a †] Fredrik Edhborg,[a †] Zachary W. Schroeder,[b] Lan Chen,[b] Michael J. Ferguson,[b] Rik R. Tykwinski[b] and Bo Albinsson[a*]

a R. Ringström, F. Edhborg, Prof. Dr. B. Albinsson
Department of Chemistry and Chemical Engineering
Chalmers University of Technology
Göteborg, Kemigården 4 SE-412 96 (Sweden)
balb@chalmers.se

b Z. W. Schroeder, L. Chen, Dr. M. J. Ferguson, Prof. Dr. R. R. Tykwinski
Department of Chemistry
University of Alberta
Edmonton, Alberta T6G 2G2 (Canada)

† These authors contributed equally

Contents

Supporting Information

Experimental Procedures

1. Synthesis of PD1–3

1.1. General Experimental

All reagents and solvents were obtained from commercial suppliers and used as received unless otherwise stated. Anhydrous solvents were obtained using a solvent purification system from LC technology solutions Inc. Purification by flash column chromatography was carried out on silica gel (SiO_2, 60 Å, 40−63 µm). Thin-layer chromatography (TLC) was carried out using commercially available aluminum sheets precoated with silica gel with fluorescence indicator and visualized under UV light at 254 and/or 360 nm. ^{1}H and ^{13}C NMR spectra were recorded on a 500 MHz Varian instrument equipped with a cold probe at 500 MHz and 126 MHz, respectively; one of the ^{1}H NMR spectra was recorded on a 700 MHz Agilent instrument. Chemical shift values are reported in ppm and coupling constants (*J*) in Hz are reported as observed. ^{1}H and ^{13}C NMR spectra are referenced against the residual solvent peak ($CDCl_3$ δ_H = 7.26 ppm, δ_C = 77.06 ppm). IR spectra were recorded on a Thermo Nicolet 8700 FTIR spectrometer and samples were measured as cast films. High-resolution mass spectrometry (HRMS) spectra were recorded on a Bruker 9.4T Apex-Qe FTICR instrument (MALDI) or a Kratos MS50G instrument (EI). Differential scanning calorimetry (DSC) measurements were made on a Perkin Elmer Pyris 1 DSC or a Mettler Toledo Polymer DSC. Thermogravimetric analyses (TGA) were made on a Perkin Elmer Pyris 1 TGA or a Mettler Toledo TGA/DSC 1. Thermal analyses were carried out under a flow of nitrogen with a heating rate of 10 °C/min. Melting points obtained from DSC analysis are reported as the peak maxima, except in cases when the sample decomposed, in which case the onset temperature of the decomposition exothermic peak is reported, as well as the exothermic maxima corresponding to the decomposition. Thermal decomposition temperature as measured by TGA (as sample weight loss) is reported as T_d in which the temperature listed corresponds to the intersection of the baseline and the tangent lines of the edge of the peak corresponding to the first significant weight loss, typically >5%. Melting points were measured on a Thomas Hoover capillary melting point apparatus.

1.2. Synthetic procedures for **1c** and **PD1**–**3**.

Compound **1a** was purchased from Alfa Aesar and used without further purification. Compounds **1b**[1] and **2**[2] were synthesized as previously reported. Compound **1c** was synthesized using a modified literature procedure.[3]

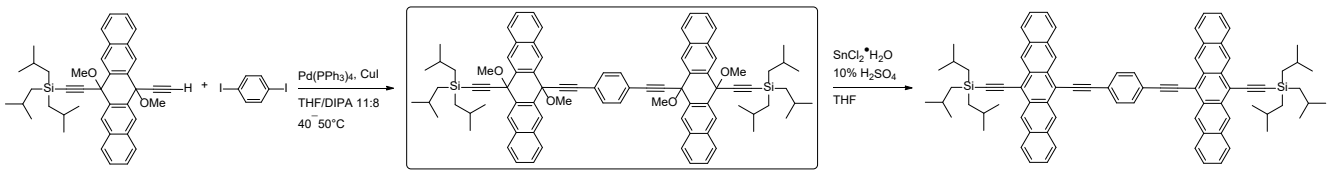

Compound PD1: This synthesis was adapted from reference [4][4]. To a solution of **2** (0.390 g, 0.665 mmol) and 1,4-diiodobenzene **1a** (0.100 g, 0.303 mmol) in N_2-sparged THF/diisopropylamine (11:8, 19 mL) was added $Pd(PPh_3)_4$ (0.035 g, 0.030 mmol) and CuI (0.003 g, 0.015 mmol). After the reaction was stirred for 21.5 h at 40–50 °C, the mixture was cooled to rt and poured into satd. aq. NH_4Cl (100 mL). H_2O (150 mL) was added, and the mixture was extracted with CH_2Cl_2 (2 x 60 mL). The combined organic phases were washed with brine (150 mL), dried over $MgSO_4$, filtered, and the solvents were removed *in vacuo*. The crude material was purified by flash column chromatography (SiO_2, CH_2Cl_2/hexanes 1:2) to afford the intermediate **M1** (0.219 g, 64%) as an off-white solid that was subject to reductive aromatization without further purification.
The intermediate **M1** (0.219 g, 0.195 mmol) was then dissolved in dry, N_2-sparged THF (12 mL), followed by addition of $SnCl_2{\cdot}2H_2O$ (0.176 g, 0.780 mmol) and 10% aq. H_2SO_4 (0.20 mL). The reaction flask was wrapped in aluminum foil to limit light exposure. The mixture was further sparged with N_2 for 2 min. The solution was stirred at rt for 3 h and then poured into MeOH (70 mL). The mixture was filtered, and the solid was washed with MeOH (5 x 15 mL). The collected solid was suspended in CH_2Cl_2 (ca. 5 mL) and stirred for 5 min, and hexanes (ca. 40 mL) were added. The suspension was filtered, and the solid was washed with hexanes to afford **PD1** (0.212 g, 97%) as a blue solid. R_f = 0.31 (SiO_2, CH_2Cl_2/hexanes 3:17). IR (cast film CH_2Cl_2) 3070 (w), 3045 (w), 2952 (s), 2923 (m), 2904 (m), 2895 (m), 2865 (m), 2118 (m), 1464 (m), 1384 (m) cm^{-1}. ^1H NMR (500 MHz, $CDCl_3$): δ 9.31 (s, 4H), 9.30 (s, 4H), 8.11–8.09 (m, 4H), 8.05 (s, 4H), 8.00–7.98 (m, 4H), 7.46–7.44 (m, 8H), 2.24 (nonet, 6H), 1.24 (d, J = 6.6 Hz, 36H), 1.01 (d, J = 6.9 Hz, 12H); ^{13}C NMR (126 MHz, $CDCl_3$) δ 132.41, 132.39, 132.0, 130.7, 130.4, 128.7, 128.6, 126.5, 126.23, 126.18, 125.9, 123.9, 118.9, 117.7, 110.3, 104.8, 104.5, 90.6, 26.7, 25.54, 25.52. MALDI HRMS (DCTB) m/z calcd for $C_{82}H_{82}Si_2$ (M^+) 1122.5950, found 1122.5963.

A crystal of **PD1** suitable for X-ray crystallographic analysis was grown at 4 °C by slow evaporation from CH_2Cl_2. X-ray data for **PD1** ($C_{82}H_{82}Si_2$), F_w = 1123.65; monoclinic crystal system; crystal dimensions 0.30 x 0.04 x 0.03 mm; space group C2/c (No. 15); a = 39.1632(9) Å, b = 5.9464(2) Å, c = 27.7746(7) Å; β = 96.8606(16)°; V = 6421.8(3) Å^3; Z = 4; $\rho_{(calcd)}$ = 1.162 g/cm^3; $2\theta_{max}$ = 140.58°; μ = 0.833 mm^{-1}; T = 173 K; total data collected = 53948; R_1 = 0.0453 [4772 independent reflections with $I \geq 2\sigma(I)$]; wR_2 = 0.1202 for 6082 data, 0 restraints, and 379 variables; largest difference, peak and hole = 0.279 and –0.263 e Å^{-3}. Data were collected with the detector set at three different positions. Low-angle (detector 2θ = –33º) data frames were collected using a scan time of 5 s, medium-angle (detector 2θ = 75º) frames using a scan time of 15 s, and high-angle (detector 2θ = 117º) frames using a scan time of 45 s. CCDC 2099715.

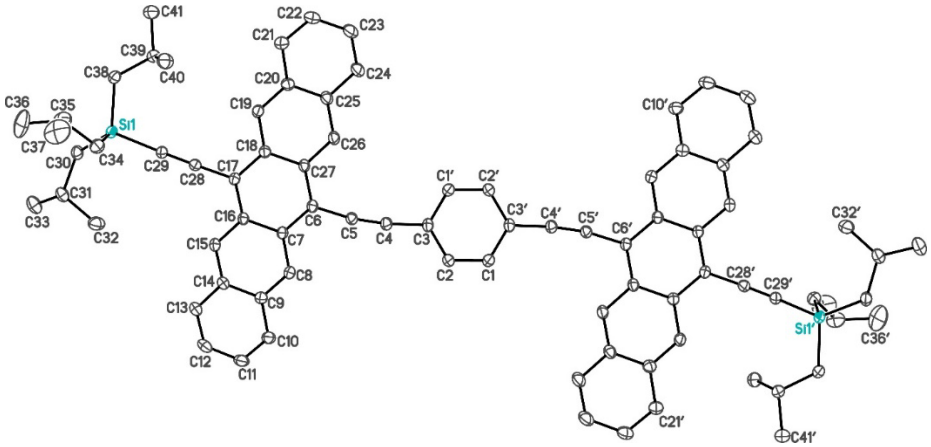

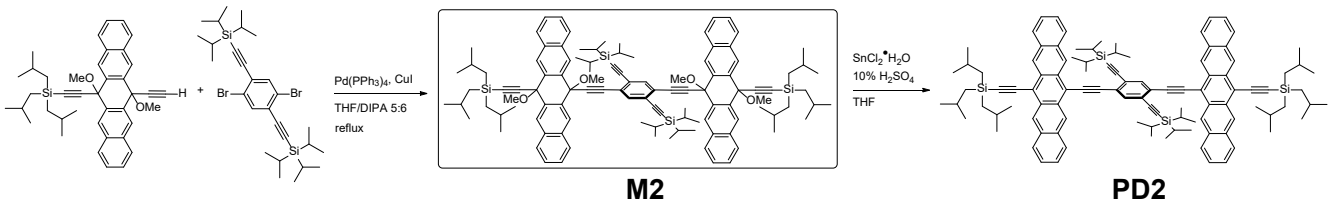

M2 **PD2**

Compound PD2: A flask charged with **1b** (323 mg, 0.542 mmol), **2** (700 mg, 1.19 mmol), and $Pd(PPh_3)_4$ (16.3 mg, 0.0141 mmol) was subjected to vacuum/N_2-purging (three cycles), and a degassed solution of THF/diisopropylamine (5:6, 22 mL) was then added. The reaction mixture was further sparged with N_2 for 10 min, and CuI (5.15 mg, 0.0271 mmol) was then added. The reaction mixture was stirred under reflux for 4 days, cooled to rt, poured into satd. aq. NH_4Cl (150 mL), and extracted with CH_2Cl_2 (2 x 50 mL). The combined organic phases were washed with H_2O (100 mL) and brine (100 mL), dried over $MgSO_4$, filtered, and concentrated *in vacuo*. The crude material (R_f = 0.54, SiO_2, CH_2Cl_2/hexanes 1:3) was purified by flash column chromatography (SiO_2, CH_2Cl_2/hexanes 1:5) to afford the intermediate **M2** (≥97% purity by ^1H NMR spectroscopy) as a pale green solid. The solid was subject to reductive aromatization without further purification. To a solution of the crude **M2** (526 mg, 0.327 mmol) in dry, N_2-sparged THF (20 mL) was added $SnCl_2{\cdot}2H_2O$ (295 mg, 1.31 mmol) and 10% aq. H_2SO_4 (1.00 mL) respectively, and the reaction mixture was sparged with N_2 for 2 min. The reaction flask was wrapped in aluminum foil to limit light exposure. After the reaction was stirred for 4 h at rt, the mixture was concentrated *in vacuo*, and the product was purified by flash column chromatography (SiO_2, CH_2Cl_2/hexanes 1:4). Removal of solvents afforded **PD2** (265 mg, 33% yield over two steps from **1b**) as a dark blue solid. R_f = 0.50 (SiO_2, CH_2Cl_2/hexanes 1:9). Mp = no melt was observed ≤ 300 °C. IR (cast film CH_2Cl_2) 3050 (w), 2952 (s), 2893 (m), 2866 (s), 2190 (w), 2158 (w), 2127 (w), 1468 (s) cm^{-1}. UV-vis (CH_2Cl_2): λ_{max} (ε) 272 (130 000), 311 (507 000), 383 (17 400), 403 (23 200), 440 (10 100), 558 (11 100), 605 (27 900), 657 (52 200). ^1H NMR (500 MHz, $CDCl_3$) δ 9.32 (s, 8H), 8.14 (s, 2H), 8.08–7.99 (m, 8H), 7.46–7.42 (m, 8H), 2.25 (nonet, J = 6.5 Hz, 6H), 1.24 (d, J = 6.5 Hz, 36H), 1.01 (d, J = 7.0 Hz, 12H), 0.83 (m, 42H); ^{13}C NMR (126 MHz, $CDCl_3$) δ 136.6, 132.40, 132.36, 130.7, 130.5, 128.9, 128.6, 126.3, 126.2, 126.1, 126.0, 125.9, 119.0, 117.7, 110.2, 104.8, 104.4, 101.7, 99.0, 93.4, 26.7, 25.54, 25.51, 18.5, 11.2 (one signal coincident or not observed). APPI HRMS *m/z* calcd. for $C_{104}H_{123}Si_4$ $(M+H)^+$ 1483.8696, found 1483.8634. TGA: Td ≈ 418 °C. DSC: decomposition, 270 (onset), 273 °C (peak).

A crystal of **PD2** suitable for X-ray crystallographic analysis was grown at ca. 4 °C in the refrigerator by slowly evaporation of a CH_3CN/CH_2Cl_2 solution (1:1 v/v). X-ray data for **PD2** ($C_{104}H_{122}Si_4{\bullet}2CH_2Cl_2$), F_w = 1654.22; monoclinic crystal system; space group $P2_1/c$ (No. 14); a = 8.3982(6) Å, b = 34.669(2) Å, c = 16.6828(9) Å; β = 90.028(4)°; V = 4857.3(5) $Å^3$; Z = 2; $\rho_{(calcd)}$ = 1.131 g/cm^3; 2θ_{max} = 144.55°; m = 1.913 mm^{-1}; T = 173 K; total data collected = 56514; R_1 = 0.0753 [9420 independent reflections with $I \geq 2\sigma(I)$]; wR_2 = 0.2281 for 9420 data, 70 restraints and 571 parameters; largest difference, peak and hole = 0.345 and –0.630 e $Å^{-3}$. The Si–C14A/B and Si–C17A/B distances (of the disordered isopropyl groups) were restrained to be approximately the same by use of the *SHELXL* **SADI** instruction. Likewise, the C–C distances of the disordered *iso*propyl groups were restrained using **SADI**. Finally, the rigid-bond restraint (**RIGU**) was applied to the anisotropic displacement parameters of the carbon atoms of the disordered *iso*propyl groups. CCDC 2099716.

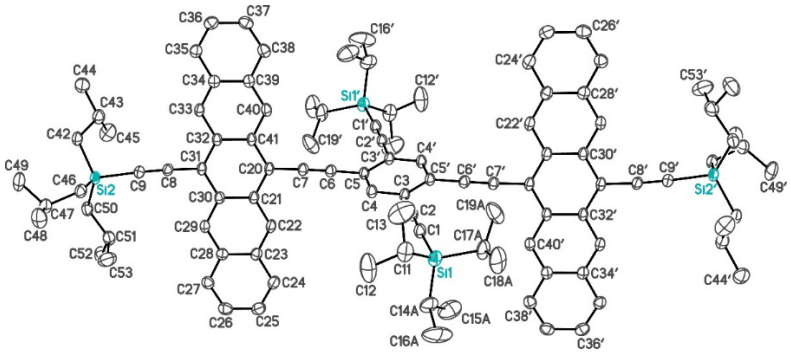

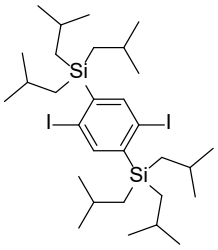

Compound 1c: This synthesis was adapted from reference [3]. To a solution of *p*-diiodobenzene (8.00 g, 24.2 mmol) in THF (60 mL) cooled to –78 °C was added tri-*iso*-butylchlorosilane (12.5 g, 14.3 mL, 53.4 mmol). Subsequently, lithium diisopropylamide (LDA) was added dropwise and the resulting mixture stirred at –78 °C for 1 h. The reaction was quenched via the addition of satd. aq. NH_4Cl (100 mL) and H_2O (25 mL) was added to dissolve inorganic solid precipitates. The reaction mixture was extracted with CH_2Cl_2 (4 x 50 mL), and the combined organic phases were washed with brine (100 mL), dried over $MgSO_4$, filtered, and concentrated *in vacuo*. The crude product was suspended in MeOH, cooled to –78 °C, and the precipitate was isolated by suction filtration. The solid was washed with H_2O (50 mL) and cold MeOH (2 x 10 mL) to afford the title compound **1c** (9.85 g, 56%) as a white solid. R_f = 0.76 (SiO_2, hexanes). Mp = 159–161 °C. IR (cast film CH_2Cl_2): 3053 (w), 2953 (s), 2927 (s), 2905 (s), 2866 (s), 1462 (m) cm^{-1}. ^1H NMR (700 MHz, $CDCl_3$) δ 7.74 (s, 2H), 1.78 (nonet, J = 7.0 Hz, 6H), 0.99 (d, J = 6.3 Hz, 12H), 0.89 (d, J = 7.0 Hz, 36H). ^{13}C NMR (126 MHz, $CDCl_3$) δ 148.4, 148.0, 105.8, 26.3, 24.9, 22.8. EI MS m/z 724.2 (M^+, 1), 669.1 ([M–Bu]$^+$, 88), 613.1 ([M–2Bu]$^+$, 100). EI HRMS *m/z* calcd for $C_{30}H_{56}I_2Si_2$ (M^+) 726.2010, found 726.1992.

Note: LDA was freshly prepared by adding *n*HexLi (2.3 M in hexanes, 21.1 mL, 48.5 mmol) to a –78 °C solution of diisopropylamine (7.53 mL, 5.40 g, 53.4 mmol) in THF (12 mL) at –78 °C. The solution of LDA was then warmed slowly to rt prior to use.

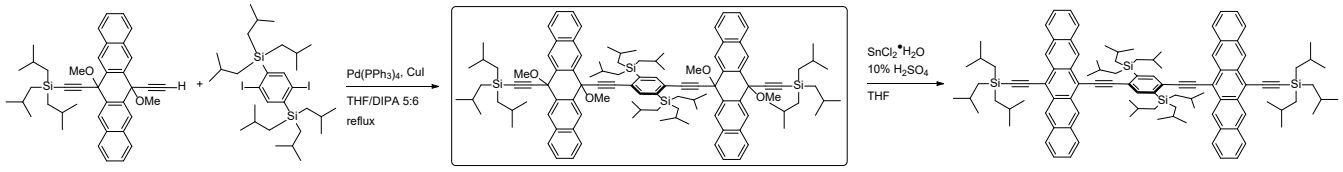

M3 **PD3**

Compound PD3: A flask charged with **1c** (393 mg, 0.541 mmol), **2** (700 mg, 1.19 mmol), $Pd(PPh_3)_4$ (62.5 mg, 0.0541 mmol) was subjected to vacuum/N_2-purging (three cycles), and a degassed solution of THF/diisopropylamine (5:6, 22 mL) was added. The reaction mixture was further sparged with N_2 for 10 min and CuI (5.15 mg, 0.0271 mmol) then added. After the reaction was stirred under reflux for 117 h, the reaction mixture was poured into satd. aq. NH_4Cl (150 mL) and extracted with CH_2Cl_2 (3 x 50 mL). The combined organic phases were washed with H_2O (100 mL) and brine (100 mL), dried over $MgSO_4$, filtered, and concentrated *in vacuo*. The crude material was purified by flash column chromatography (SiO_2, CH_2Cl_2/hexanes 1:5 → 1:4) to afford the intermediate **M3** (291 mg, ≥97% purity by ^{1}H NMR spectroscopy) as a pale green solid. The solid was then subject to reductive elimination without further purification. To a solution of **M3** (206 mg, 0.125 mmol) in dry, N_2-sparged THF (9 mL) was added $SnCl_2{\cdot}2H_2O$ (113 mg, 0.501 mmol) and 10% aq. H_2SO_4 (0.50 mL) respectively, and sparged with N_2 for 2 min. The reaction flask was wrapped in aluminum foil to limit light exposure. After the reaction stirred for 4 h at rt, the mixture was concentrated *in vacuo* and the product was purified by column chromatography (SiO_2, CH_2Cl_2/hexanes 1:20 → 1:16). The removal of solvents afforded **PD3** (118 mg, 14% over two steps from **1c**) as a dark blue solid. R_f = 0.69 (SiO_2, CH_2Cl_2/hexanes 1:9). Mp = no melt was observed ≤ 300 °C. IR (cast film CH_2Cl_2): 3051 (w), 2952 (s), 2924 (m) 2895 (m), 2867 (m), 2124 (w), 1464 (m) cm^{-1}. UV-vis (CH_2Cl_2): λ_{max} (ε) 273 (63 400) 313 (554 000), 352 (24 100), 377 (26 500), 395 (51 300), 440 (9 000), 501 (4 470), 553 (sh, 9 930), 612 (27 000), 648 (46 800), 668 (47 600), 691 (35 000). ^{1}H NMR (500 MHz, $CDCl_3$) δ 9.44 (s, 4H), 9.35 (s, 4H), 8.24 (s, 2H), 8.09–8.01 (m, 8H), 7.47–7.44 (m, 8H), 2.25 (nonet, J = 6.5 Hz, 6H), 2.01 (nonet, J = 6.5 Hz, 6H), 1.35 (d, J = 7.0 Hz, 12H), 1.24 (d, J = 6.5 Hz, 36H), 1.01 (d, J = 7.0 Hz, 12H), 0.95 (d, J = 6.5 Hz, 36H). ^{13}C NMR (126 MHz, $CDCl_3$) δ 142.0, 140.1, 132.4, 132.3, 130.9, 130.6, 128.7, 128.6, 128.5, 126.6, 126.23, 126.19, 118.6, 118.4, 110.2, 106.9, 104.8, 92.9, 26.7, 26.6, 25.6, 25.5, 25.1, 23.4 (1 signal coincident or not observed). MALDI HRMS (DCTB) m/z calcd for $C_{106}H_{134}Si_4$ (M^+) 1518.9557, found 1518.9561. TGA: Td ≈ 426 °C; DSC: decomposition, 308.21 (onset), 314.78 °C (peak); 339.47 (onset), 339.90 °C (peak).

A crystal of **PD3** suitable for X-ray crystallographic analysis was grown at 4 °C, by slow evaporation of a CH_2Cl_2 solution layered with MeOH. X-ray data for **PD3** ($C_{106}H_{134}Si_4$•0.65CH_2Cl_2), F_w = 1575.69; monoclinic crystal system; space group $P2_1/c$ (No. 14); a = 8.0655(3) Å, b = 14.6582(5) Å, c = 41.1040(12) Å; β = 91.616(2)°; V = 4857.6(3) Å^3; Z = 2; $\rho_{(calcd)}$ = 1.077 g/cm^3; $2\vartheta_{max}$ = 140.64°; μ = 1.222 mm^{-1}; T = 173 K; total data collected = 70805; R_1 = 0.0520 [9154 independent reflections with $I \geq 2\sigma(I)$]; ωR_2 = 0.1413 for 9154 data, 15 restraints, and 527 variables; largest difference, peak and hole = 0.352 and –0.354 e Å^{-3}. Attempts to refine peaks of residual electron density as disordered or partial-occupancy solvent dichloromethane chlorine or carbon atoms were unsuccessful. The data were corrected for disordered electron density through use of the SQUEEZE procedure as implemented in *PLATON* (Spek, A. L. *Acta Crystallogr.* **2015**, *C71*, 9–18. *PLATON* - a multipurpose crystallographic tool; Utrecht University, Utrecht, The Netherlands). A total solvent-accessible void volume of 366 Å^3 with a total electron count of 54 (consistent with 1.3 molecules of solvent dichloromethane, or 0.65 molecules per formula unit of the target molecule) was found in the unit cell. The disordered *iso*butyl groups had the following sets of bond lengths restrained by use of the *SHELXL* **SADI** instruction: C30–C31A, C30–C31B; C31A–C32A, C31A–C33A, C31B–C32B, C31B-C33B; Si1–C38A, Si1–C38B; C38A–C39A, C38B–C39B; C39A–C40A, C39A–C41A, C39B–C40B, C39B–C41B. CCDC 2099717.

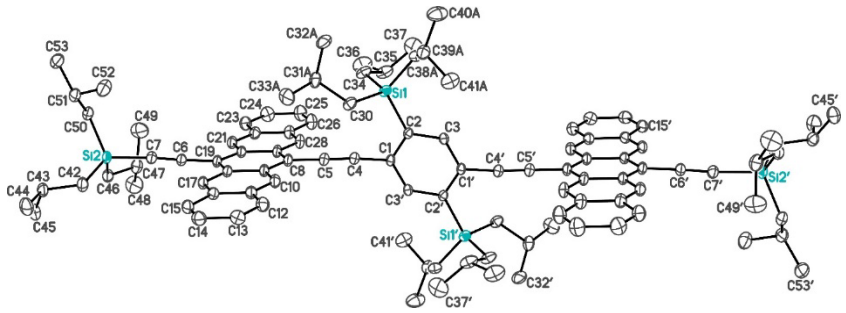

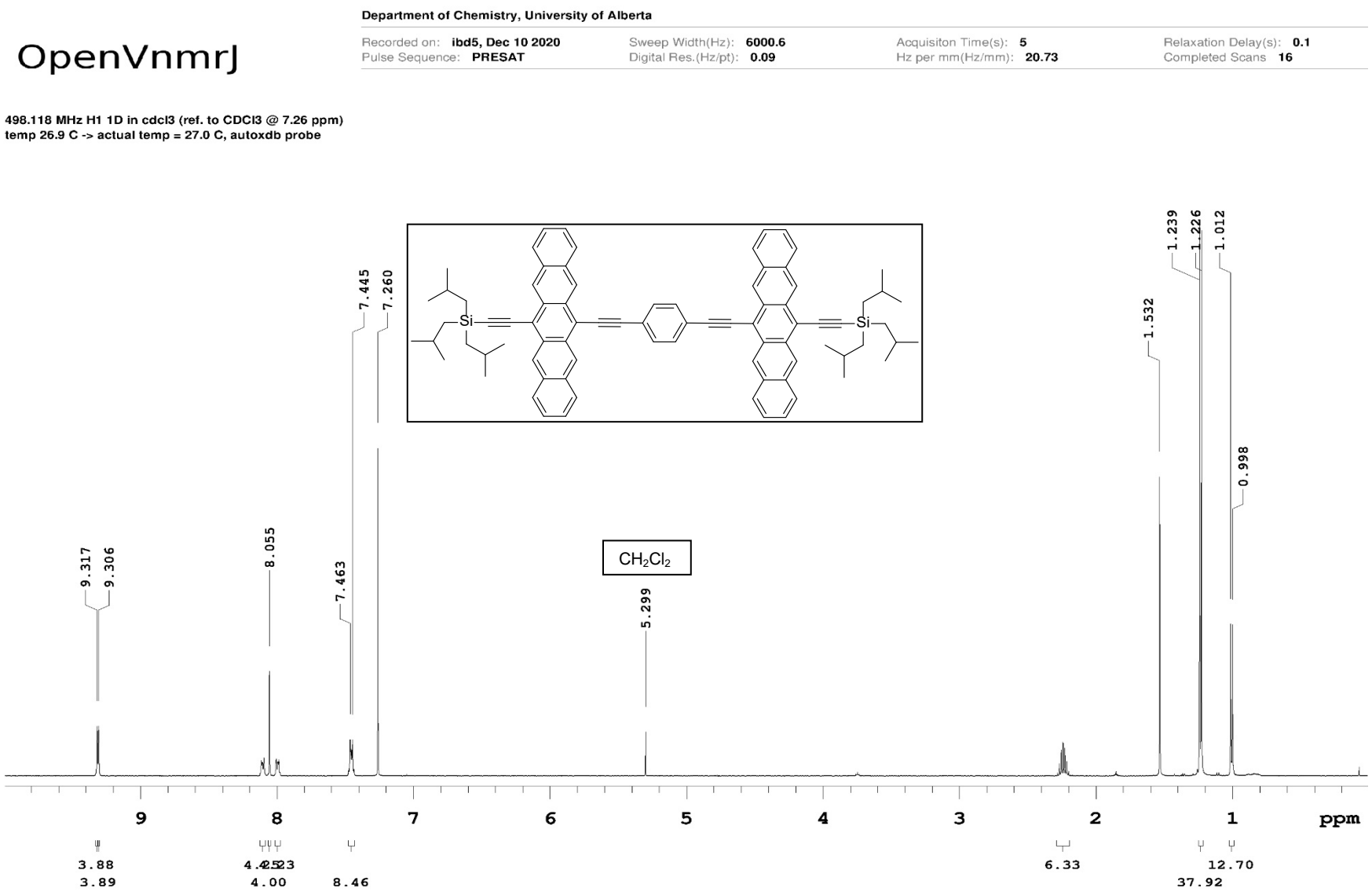

Figure S1.1. ^{1}H NMR spectrum (500 MHz) of **PD1** recorded in $CDCl_3$.

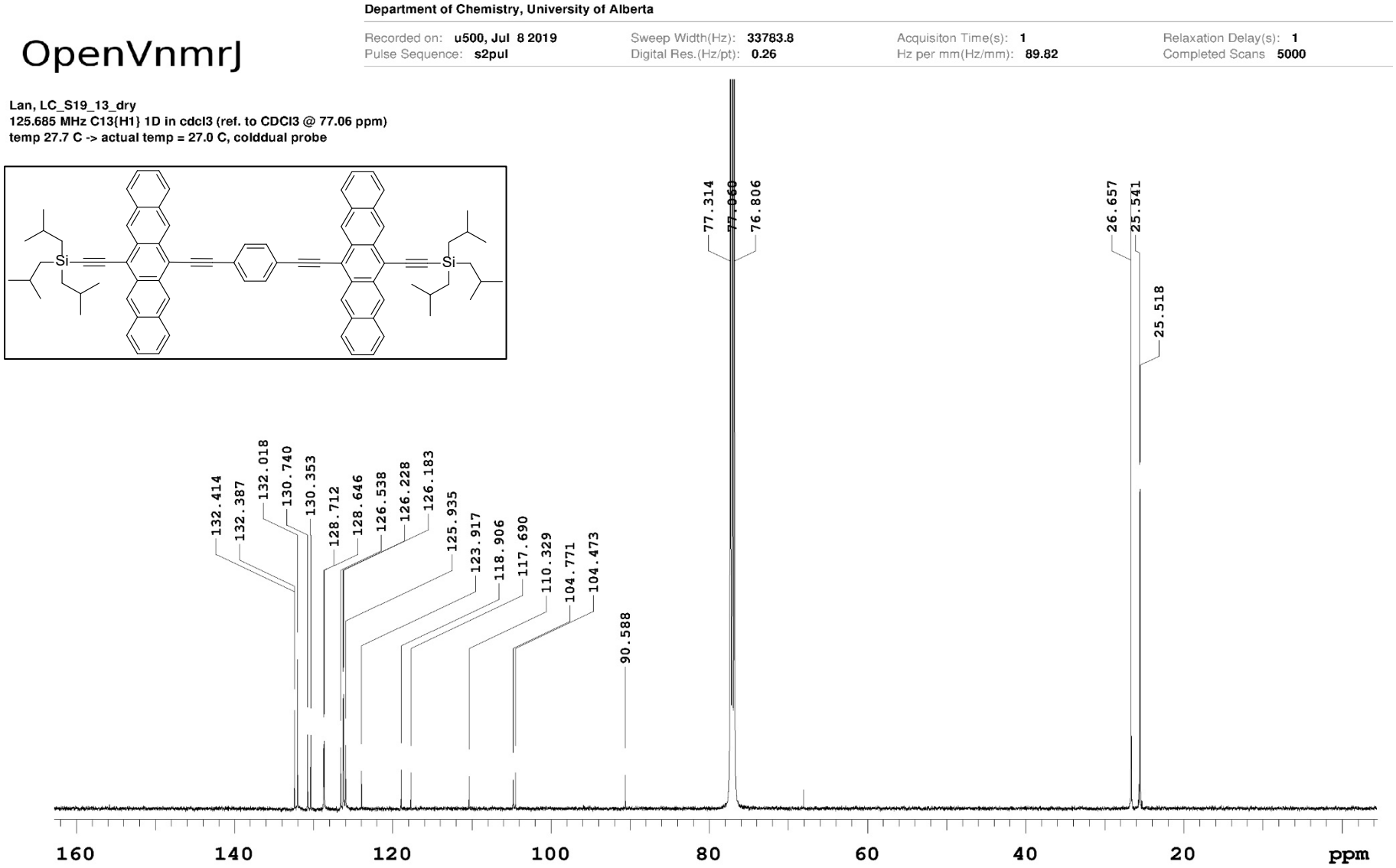

Figure S1.2. ^{13}C NMR spectrum (126 MHz) of **PD1** recorded in $CDCl_3$.

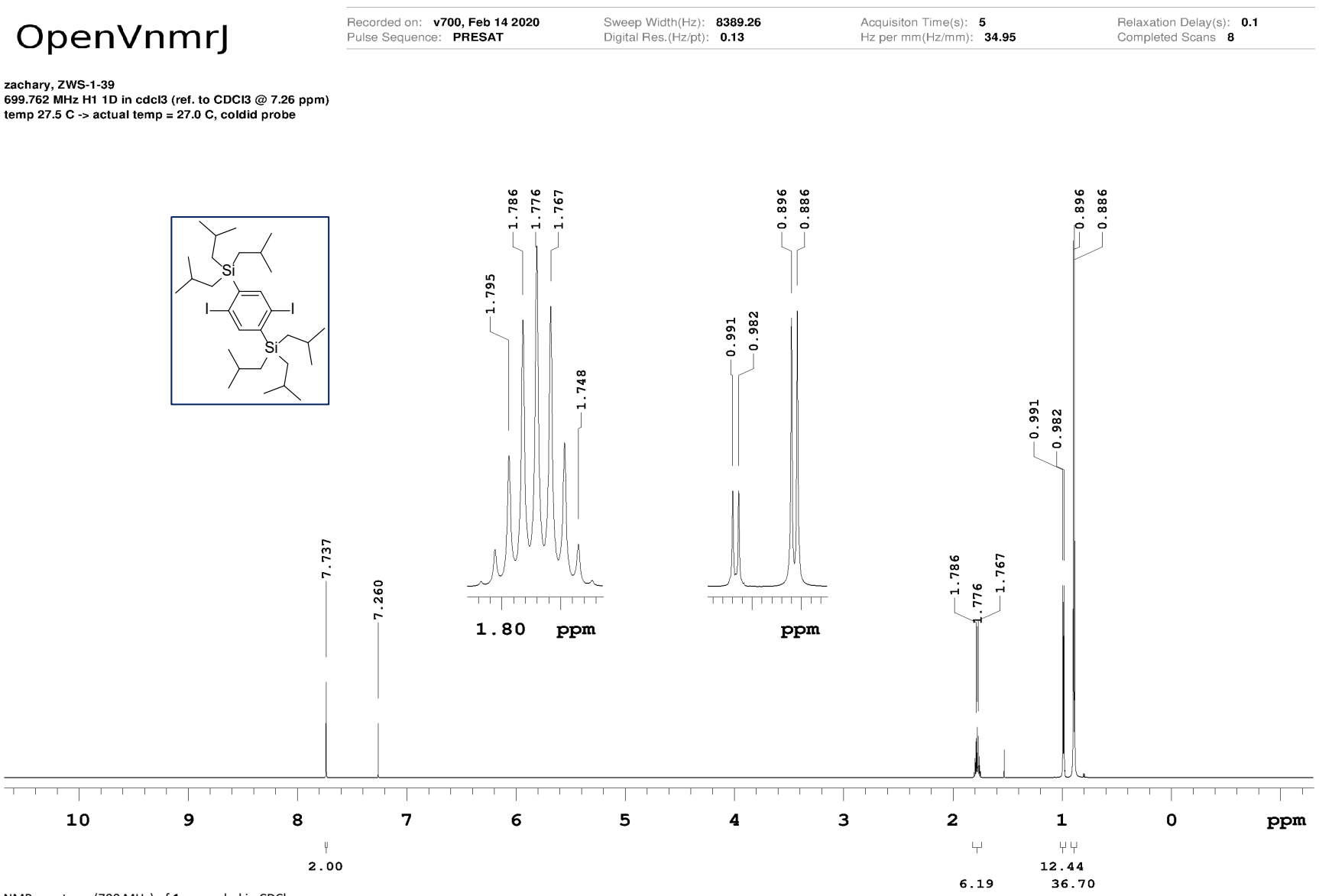

Figure S1.3. ^{1}H NMR spectrum (700 MHz) of **1c** recorded in $CDCl_3$.

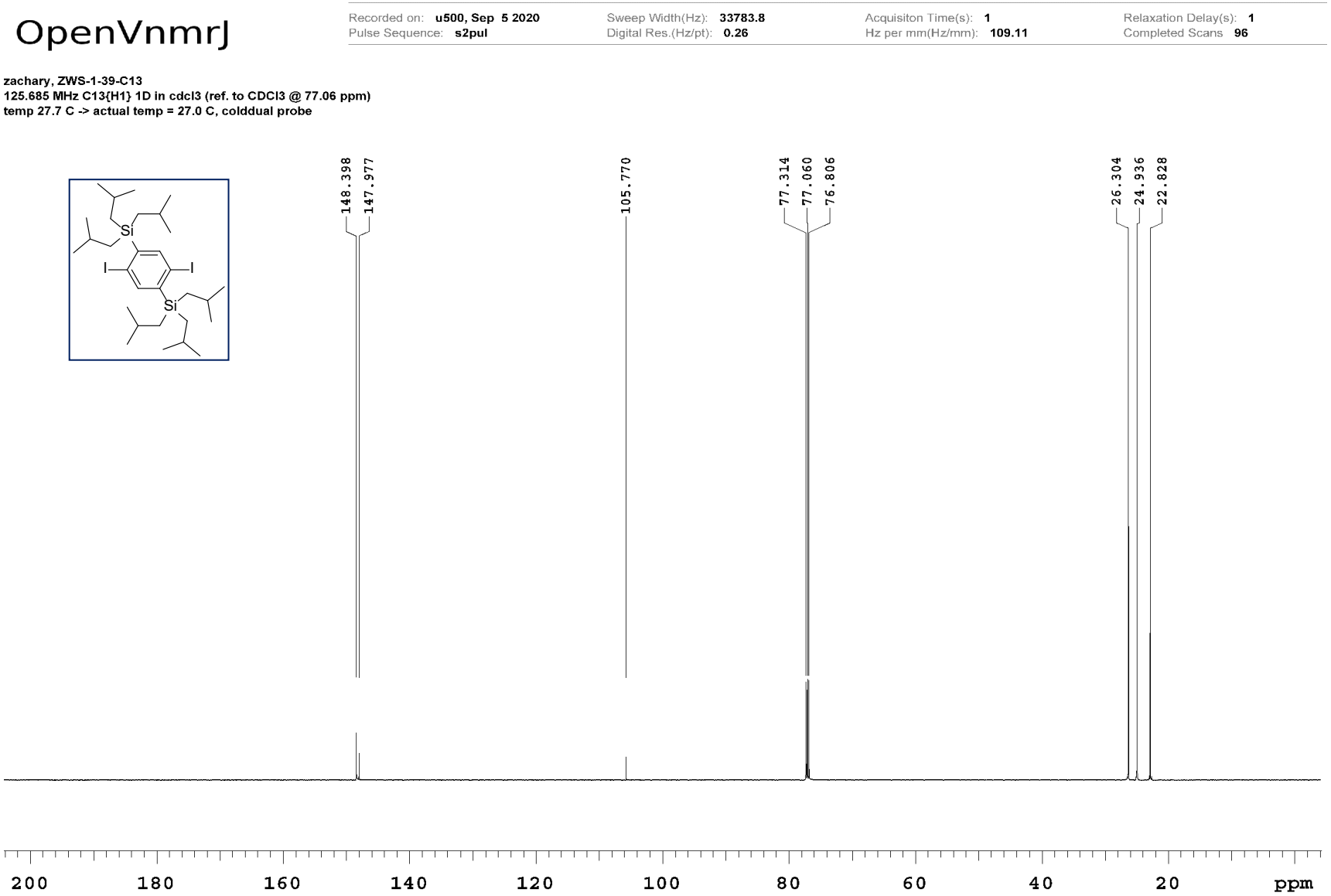

Figure S1.4. ^{13}C NMR spectrum (126 MHz) of **1c** recorded in $CDCl_3$.

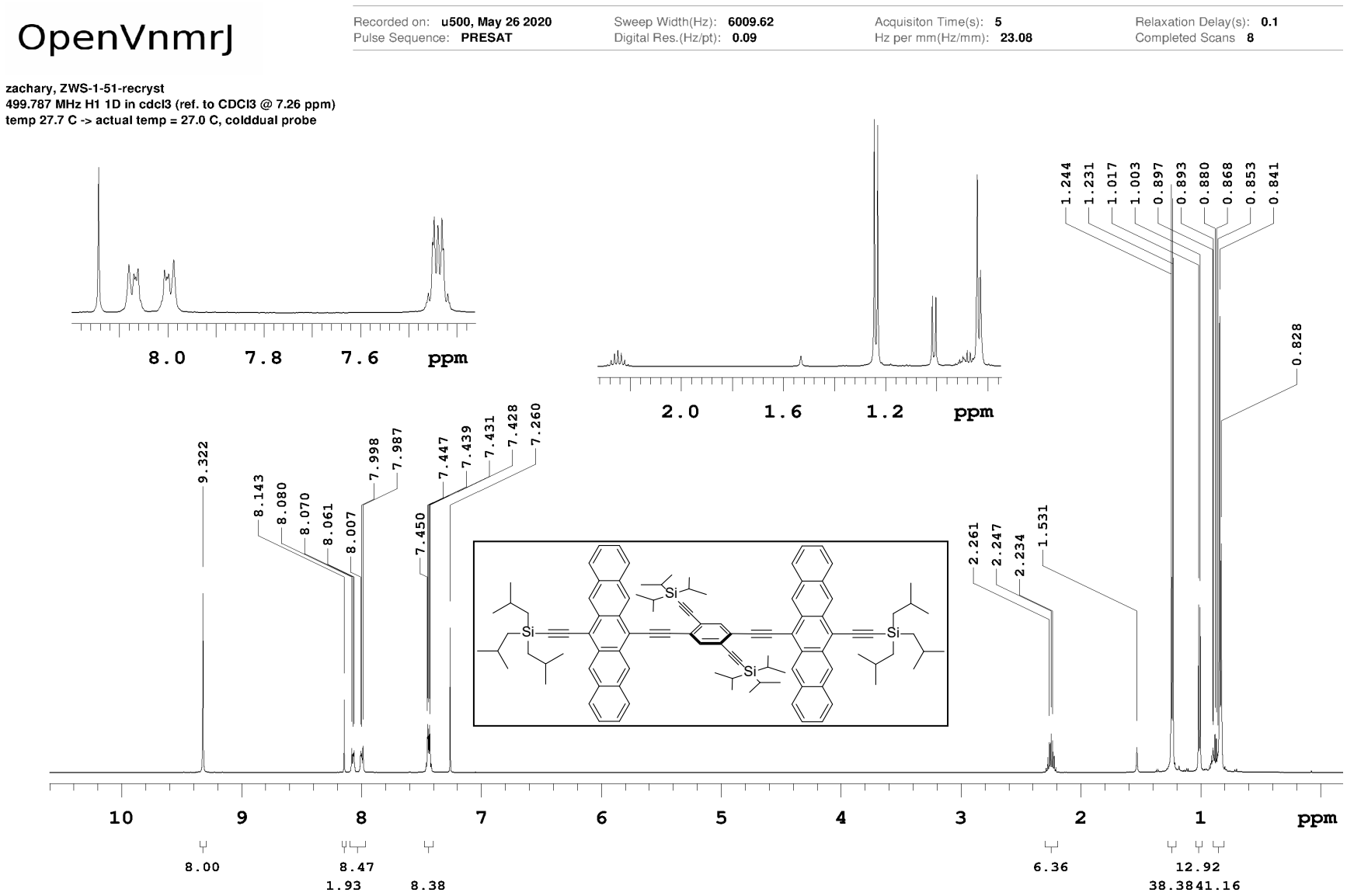

Figure S1.5. ^{1}H NMR spectrum (500 MHz) of **PD2** recorded in $CDCl_3$.

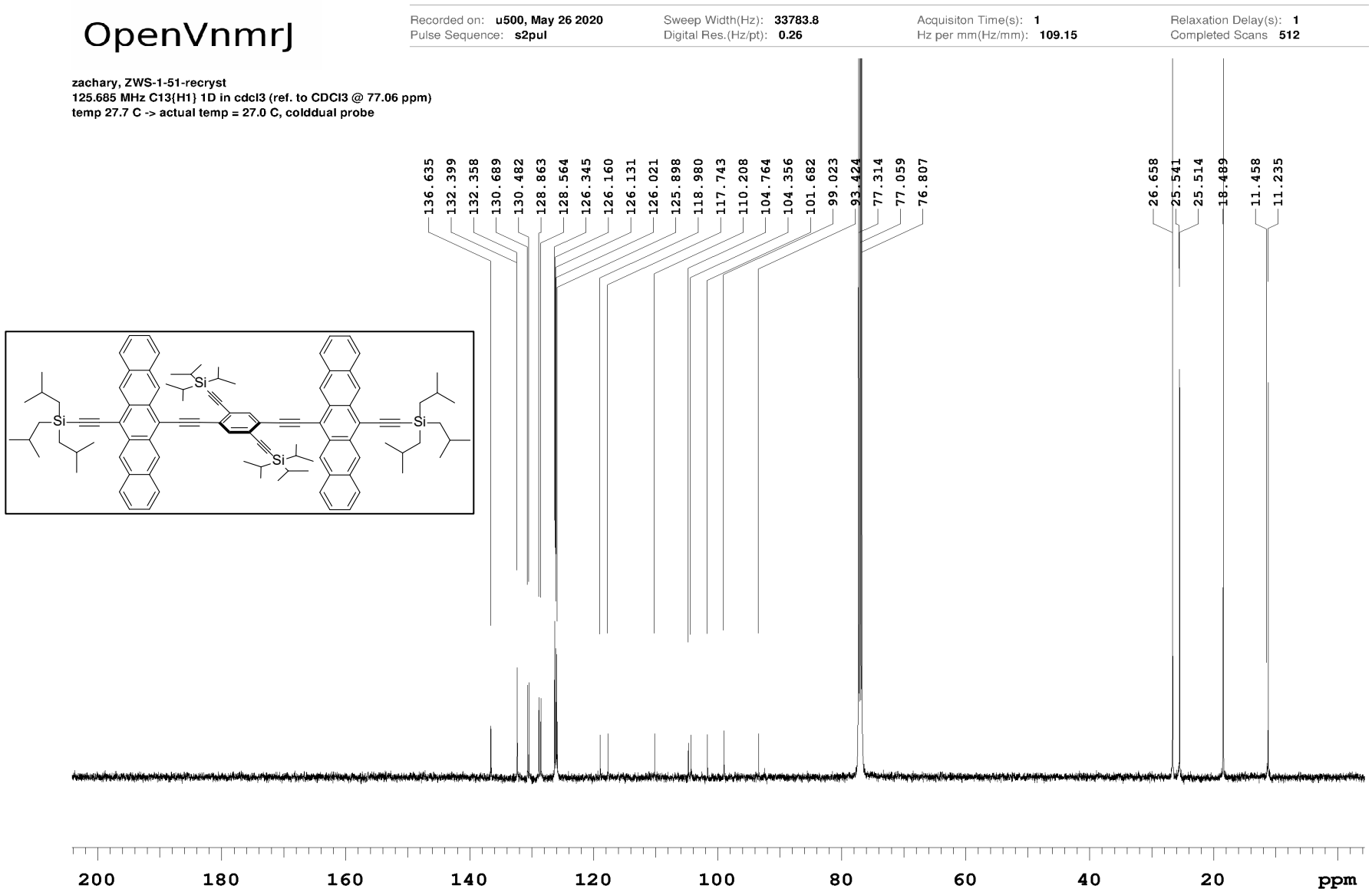

Figure S1.6. ^{13}C NMR spectrum (126 MHz) of **PD2** recorded in $CDCl_3$.

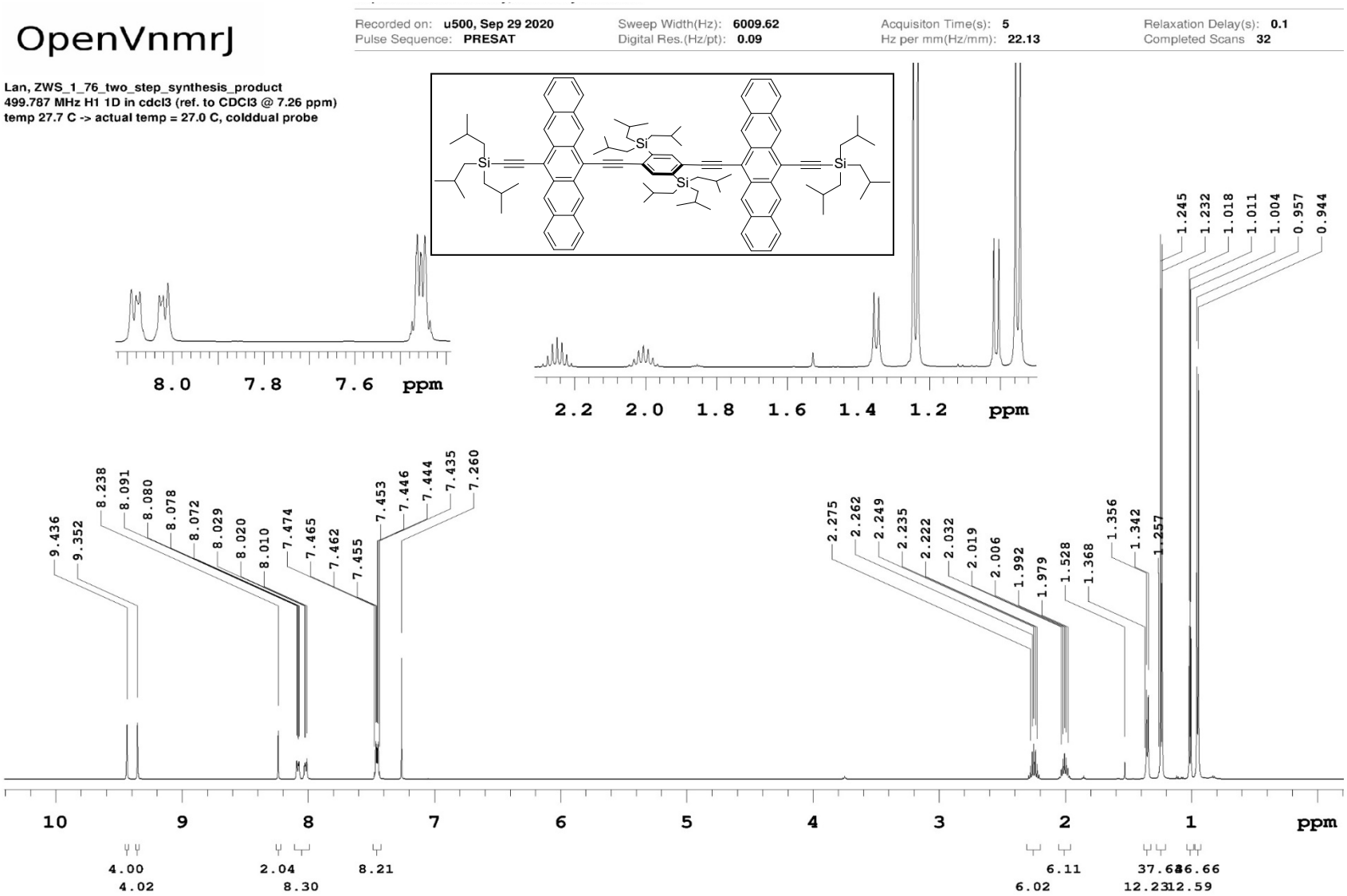

Figure S1.7. ^{1}H NMR spectrum (500 MHz) of **PD3** recorded in $CDCl_3$.

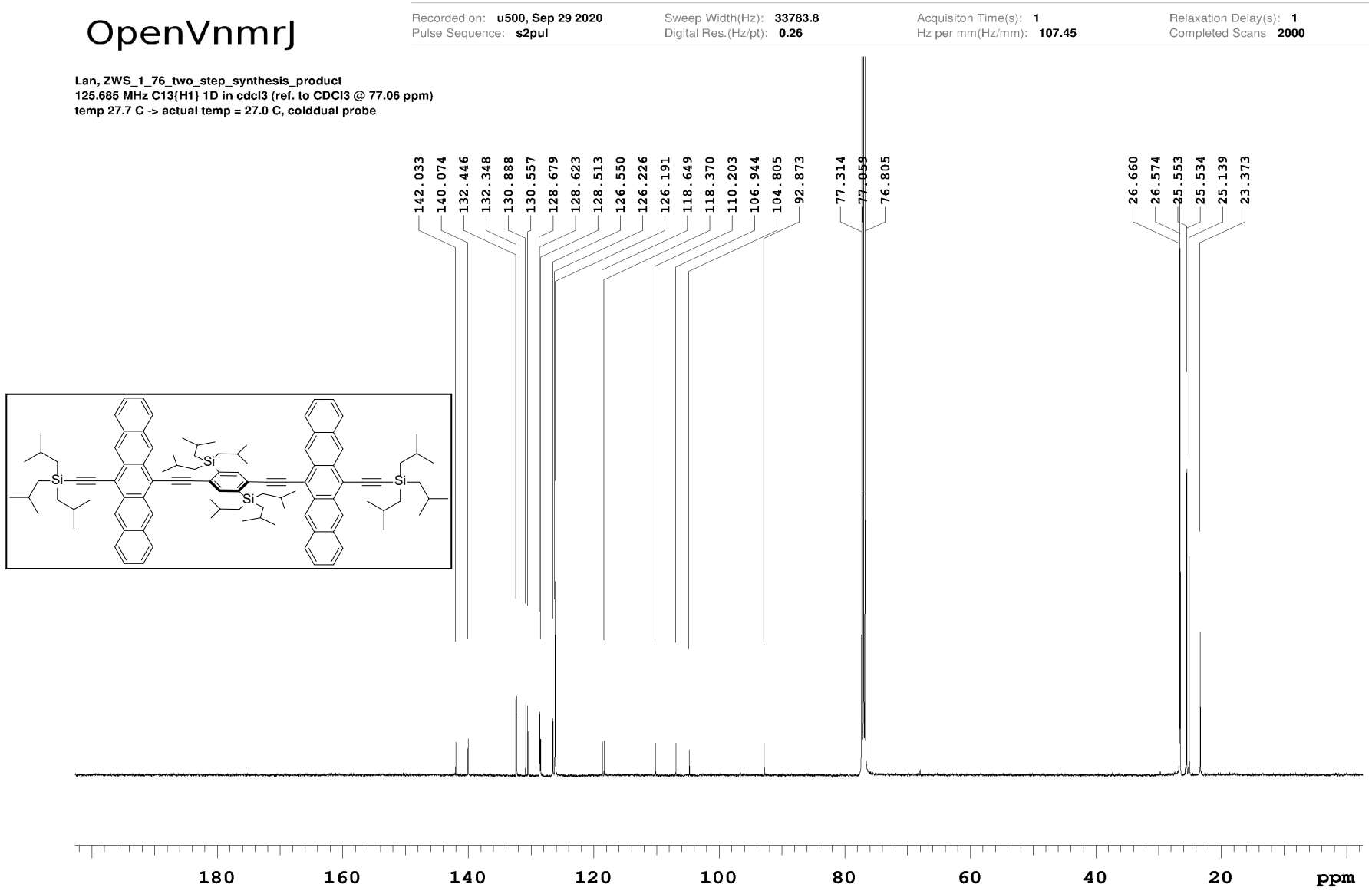

Figure S1.8. ^{13}C NMR spectrum (126 MHz) of **PD3** recorded in $CDCl_3$.

Mass Spectrometry Facility Department of Chemistry

Analysis Info

Analysis Name:	T:\Service\190712_0_K9_000001.d	Acquisition Date:	12/07/2019 1:26:58 PM
Method:	MALDI_DCTB_1k_new	Instrument:	apex-Qe
Sample Name:	LC_19S_13	Operator:	
Comment:	L. Chen, R. Tykwinski, DCTB as matrix, 9.4T FTICR MS		

Acquisition Parameter

Ionisation Mode: Positive MALDI Mode: n/a

Generate Molecular Formula Parameter

Formula, min.:	C74						
Formula, max.:	C82H82Si2N0O0						
Measured m/z:	1122.6			Charge:	1	Tolerance: 2	ppm
Check Valence:	no	Min.:	0	Max.:	0		
Nitrogen Rule:	no						
Filter H/C Ratio:	no	Min.:	0	Max.:	3		
Estimate # of C:	yes					Electron Configuration:	both

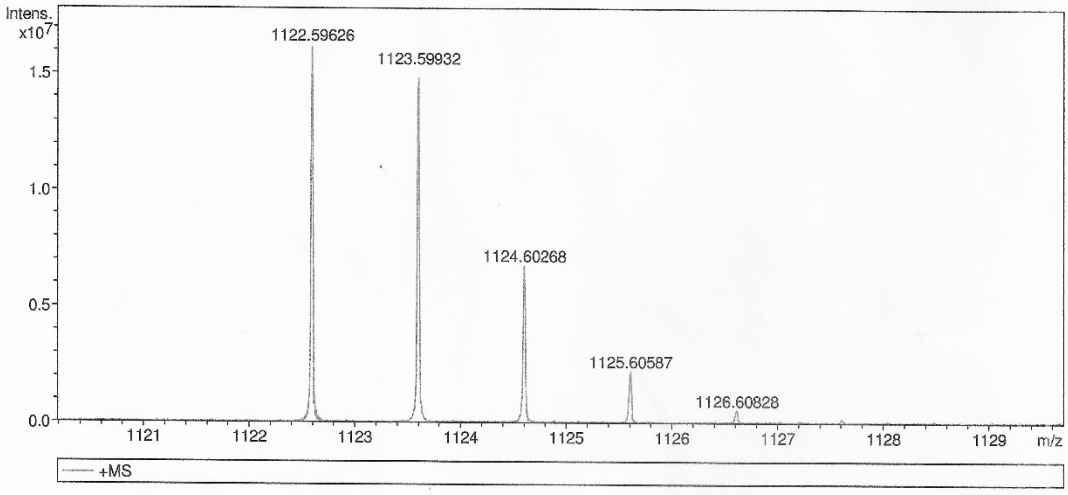

Sum Formula	Sigma	m/z	Err [ppm]	Mean Err [ppm]	Err [mDa]	rdb	N Rule	e⁻
C 82 H 82 Si 2	0.073	1122.59496	-1.16	-1.68	-1.30	44.00	ok	odd

Bruker Daltonics DataAnalysis 3.4 printed: 12/07/2019 2:44:39 PM Page 1 of 1

Figure S1.9. HRMS expansion of **PD1**.

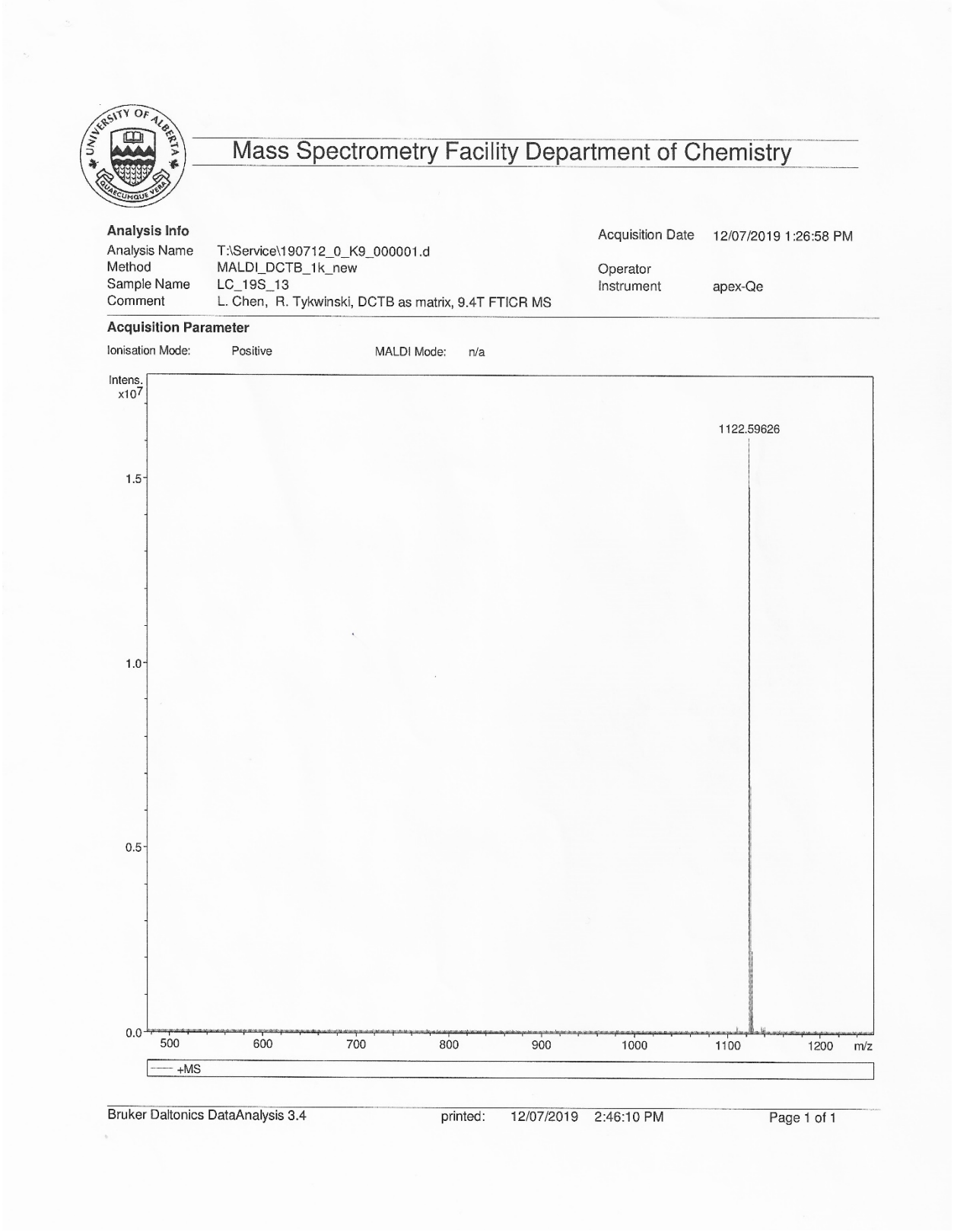

Figure S1.10. HRMS of **PD1**.

Sample Name	TIPS-Alkyne-linker-d	**Position**	-1	**Instrument Name**	oaTOF6220	**User Name**	Béla
Inj Vol	5	**InjPosition**		**SampleType**	Sample	**IRM Calibration Status**	Success
Data Filename	20052809.d	**ACQ Method**		**Comment**	Z. Schroeder, Tykwinski	**Acquired Time**	5/28/2020 12:18:34 PM

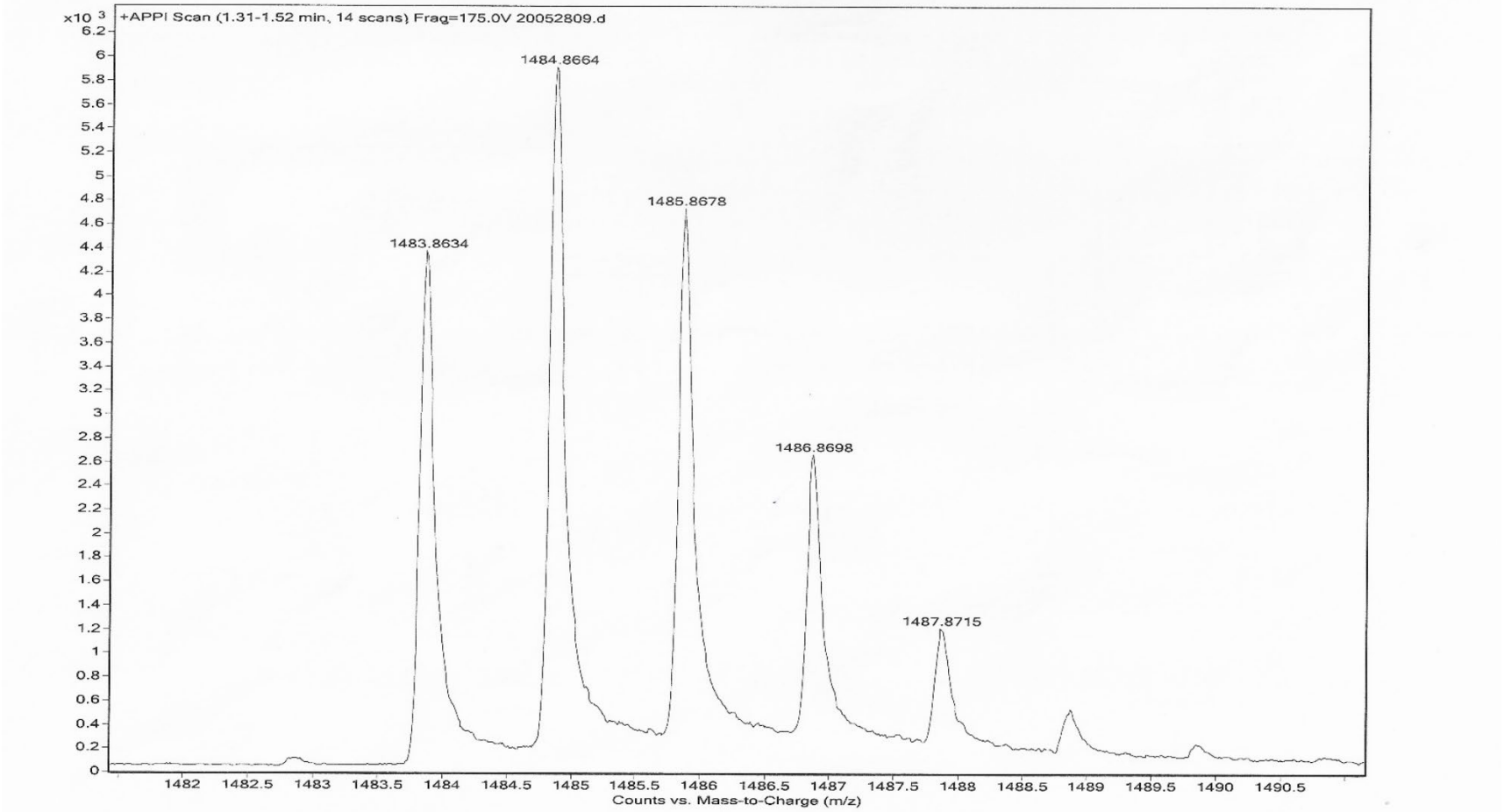

Figure S1.11. HRMS expansion of **PD2**.

Qualitative Analysis Report

Data Filename	20052809.d	**Name**	Z. Schroeder, Tykwinski
Sample Name	TIPS-Alkyne-linker-dimer	**Position**	-1
Instrument Name	oaTOF6220	**Operator**	Béla
Acq Method		**DA Method**	DA_FIA.m

User Spectra

Fragmentor Voltage	Collision Energy	Ionization Mode
175	0	Appi

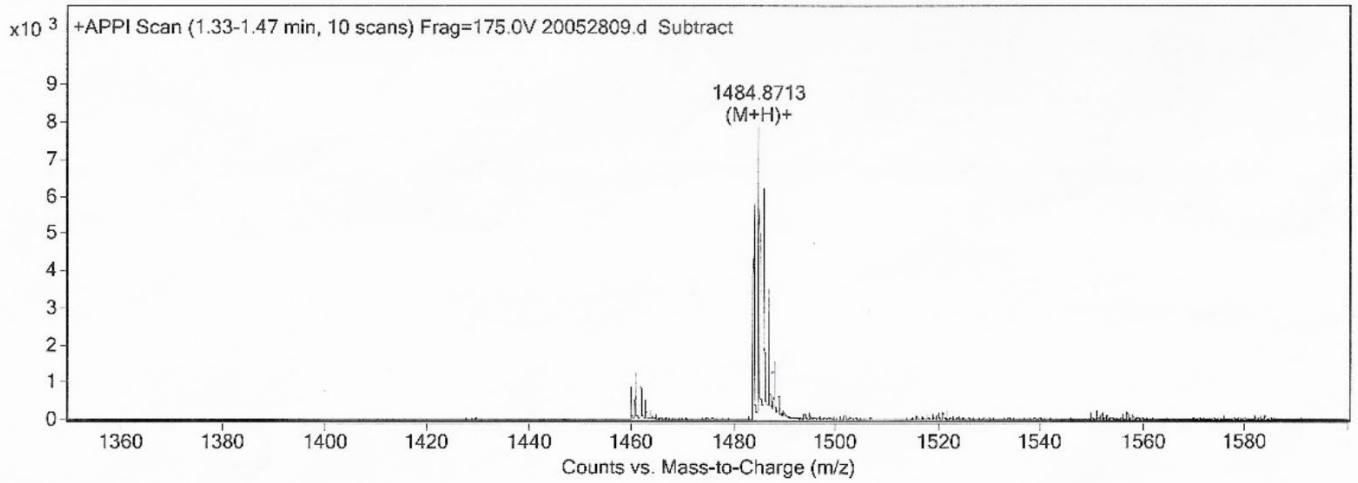

Formula Calculator Results

Formula	Ion Species	Mass	Calc Mass	m/z	Calc. m/z	Diff (mDa)	Diff (ppm)	DBE	Score
C104 H122 Si4	C104 H123 Si4	1482.8611	1482.8624	1483.8682	1483.8696	1.24	0.84	48	98.51

Figure S1.12. HRMS of **PD2**.

Mass Spectrometry Facility Department of Chemistry

Analysis Info

Analysis Name:	T:\Service\201030_0_I2_000001.d	Acquisition Date:	30/10/2020 3:34:23 PM
Method:	MALDI_DCTB_1k_new	Instrument:	apex-Qe
Sample Name:	ZWS_1_76	Operator:	
Comment:	L. Chen, R. Tykwinski, DCTB as matrix, 9.4T FTICR MS		

Acquisition Parameter

Ionisation Mode: Positive MALDI Mode: n/a

Generate Molecular Formula Parameter

Formula, min.:	C98						
Formula, max.:	N0O0Si4						
Measured m/z:	1518.96			Charge:	1	Tolerance:	2 mDa
Check Valence:	yes	Min.:	0	Max.:	100		
Nitrogen Rule:	no						
Filter H/C Ratio:	no	Min.:	0	Max.:	3		
Estimate # of C:	yes					Electron Configuration:	both

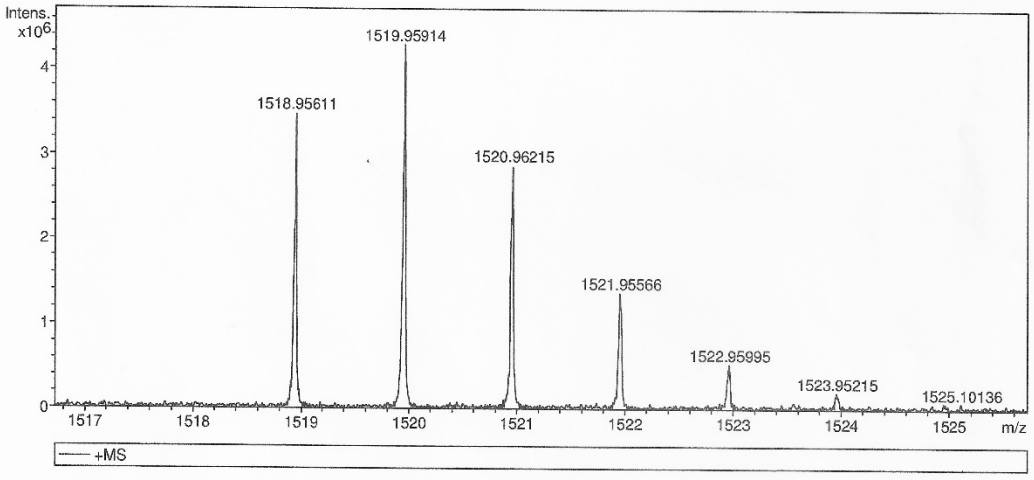

Sum Formula	Sigma	m/z	Err [ppm]	Mean Err [ppm]	Err [mDa]	rdb	N Rule	e⁻
C 106 H 134 Si 4	0.068	1518.95571	-0.26	0.31	-0.40	44.00	ok	odd

Bruker Daltonics DataAnalysis 3.4 printed: 02/11/2020 9:09:26 AM Page 1 of 1

Figure S1.13. HRMS expansion of **PD3**.

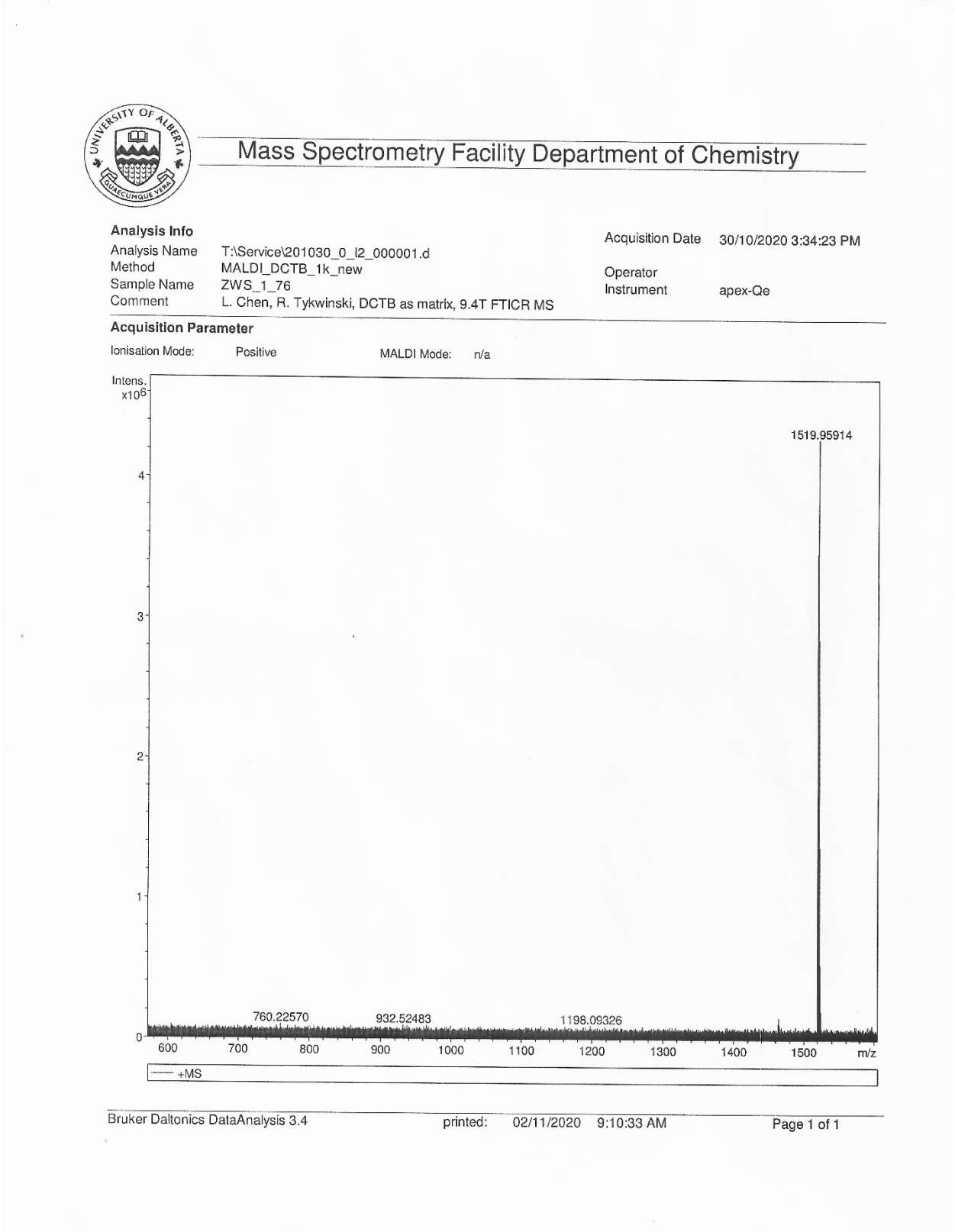

Figure S1.14. HRMS of **PD3**.

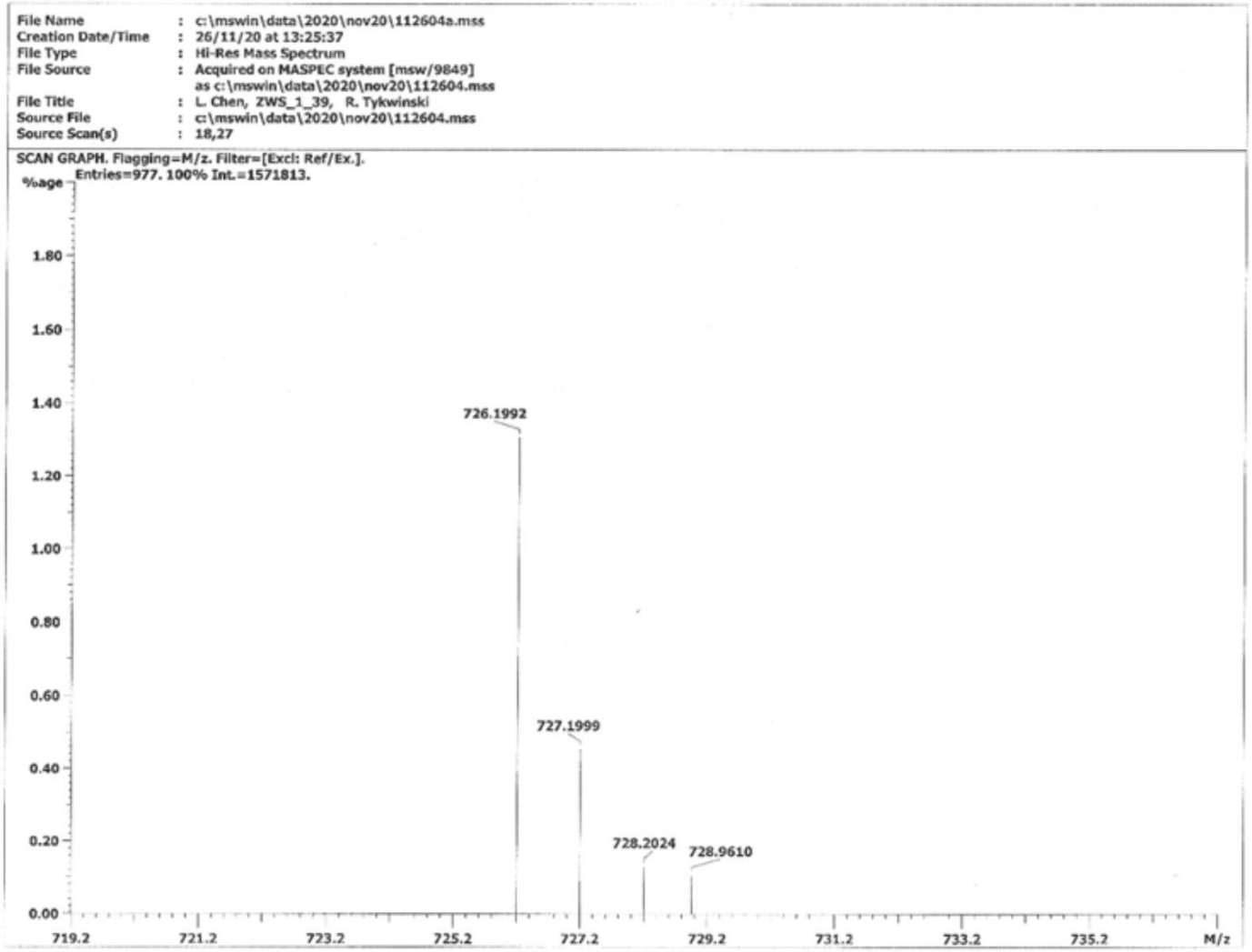

Figure S1.15. HRMS expansion of **1c**.

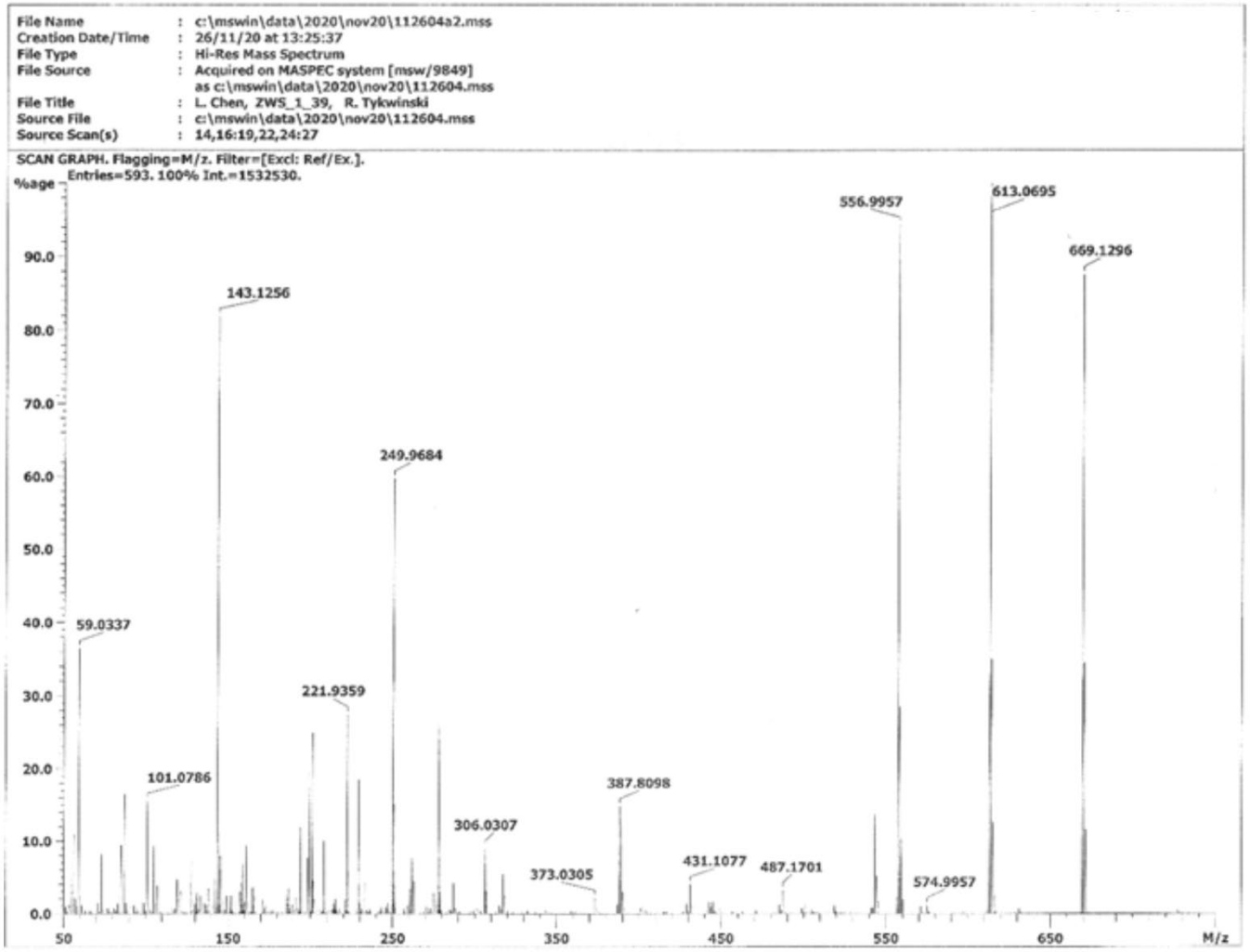

Figure S1.16. HRMS of **1c**.

2. Spectroscopic and computational details

Steady state absorption measurements were recorded with Varian-Cary 50 Bio and 4000 spectrophotometers. The emission spectra were obtained with a Spex Fluorolog 3 spectrofluorometer from JY Horiba.

Femtosecond transient absorption (fsTA). A Ti:sapphire oscillator (Tsunami, Spectra Physics) was used as seed to a Ti:sapphire regenerative amplifier (Spitfire, Spectra Physics) pumped by a frequency-doubled diode-pumped Nd:YLF laser (Evolution-X,Spectra Physics). This produced pulses of around 200 fs duration (fwhm) at a 1 kHz repetition rate; the 800 nm output from the amplifier was split, and the two beams were used as pump and probe light. An optical parametric amplifier (TOPAS, Light Conversion Ltd.) was used to tune the pump wavelength to yield the appropriate excitation wavelengths (1μJ/pulse at the sample). The probe light was focused on a rotating CaF_2 plate to generate a supercontinuum, and the pump beam was delayed with respect to the probe beam with an optical delay stage (range 0−10 ns). The supercontinuum was split into a probe and reference beam, and the probe beam was overlapped with the pump at the sample. Residual fundamental was dumped using an 800 nm notch filter. The transmitted probe and reference beam were directed to optical fibers and detected by a CCD camera (iXon-Andor) operating synchronously with the 1 kHz laser. The transient spectra were obtained from the difference of the probe light divided by the reference with and without excitation of the sample by the pump beam; 2000 spectra were averaged per delay time using a home written LabVIEW program controlling the setup. The polystyrene matrix samples were continuously moved during the measurements and the samples at cryogenic temperature were moved at even intervals to ensure minimal degradation by exposing different parts of the sample to the intense pump pulse. Pump and probe beam overlap in the cryostat was achieved by initially overlapping the beams in a 2 mm cuvette. The cuvette was subsequently replaced with the cryostat in the exact same position and adjustments were made to correct for the refractions caused by the cryostat quartz windows. All transient absorption measurements in solution were performed with a concentration of approximately 30 μM.

Nanosecond transient absorption (nsTA) spectra were recorded using an Edinburgh Instrument LP 980 spectrometer with a CCD camera (CCD, Andor DH320T-25F-03).

Cryogenic temperature measurements were performed in 2-methyltetrahydrofuran (MTHF) by using a temperature controlled liquid nitrogen cryostat (Optistat-Oxford Instrument).

Kinetic analysis. Before kinetic analysis, the fsTA raw data was chirp-corrected and the pump scatter was removed. All kinetic analysis was performed in a Python-based program (KiMoPack, https://github.com/erdzeichen/KiMoPack) written by Assoc. Prof. Jens Uhlig at Lund University, which is based on adaptations from previously published schemes.[5,6] Global analysis, i.e. the application of kinetic models in a least square fitting process, results in rate constants and their corresponding evolution associated spectra (EAS). The EAS represents the spectral components in a sequential model where the first and the second spectral component decays and rises, respectively, with the same time constant. The spectral evolution is often referred to as species associated spectra (SAS) when a more complex model involving both sequential and parallel models are combined.[6] The fittings presented herein were visually compared to the raw data and were only accepted after a good spectral and temporal match in the entire investigated wavelength region. In this study the sequential model used for the room temperature measurements in toluene and benzonitrile is of the form $S_0S_1 \rightarrow T_1T_1 \rightarrow$ ground state (GS). However, it should be noted that the EAS obtained here are essentially an average of the kinetics for the multiple conformers that are likely being excited.

Computational details. All computational analysis was performed using the Gaussian 16 program package.[7] In all calculations, the terminal silyl groups on the pentacene units were omitted and replaced with hydrogen atoms to save computational time and no solvation effects were included in the calculations.

The lowest energy conformations were calculated using the density functional theory (DFT) approximation with the B3LYP functional and the 6-31G(dp) basis set. The same functional and basis set was used in the potential energy scan over the dihedral angle between the plane of one of the pentacene units and the phenylene unit, as presented in Figure 1. In detail, the angle θ was defined as the dihedral angle between the plane formed by atom A, B, and C and the plane formed by atom B, C, and D, see Figure S2.1. The potential energy of each conformer was calculated in a relaxed optimization where the angle θ is fixed and all other atomic coordinates are allowed to relax to find the lowest energy of the system. No symmetry constraints were used.

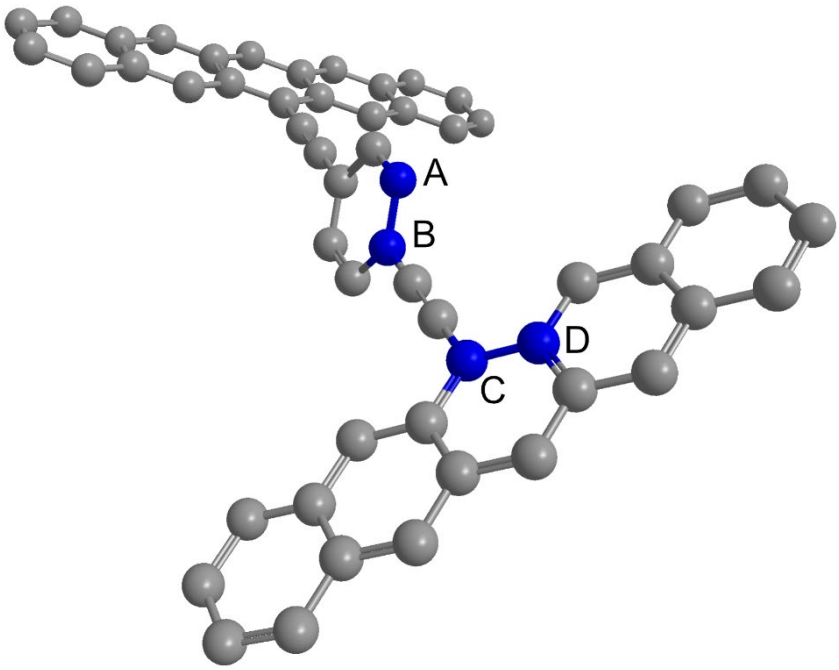

Figure S2.1. Schematic illustration clarifying the definition of the dihedral angle, θ. θ is defined as the dihedral angle between the plane formed by atom A, B, and C and the plane formed by B, C, and D.

Time dependent DFT (TD-DFT) was used with the CAM-B3LYP functional and the 6-31G(dp) basis set to calculate the electronic transition of various rotational conformers of the molecules, presented in Figure 6. The CAM-B3LYP functional was chosen because it has been shown to accurately describe the lowest electronic transition ($S_0 \rightarrow L_a$) in acenes.[8] In these calculations, a model system with the molecular structure of **PD1** (without terminal silyl substituents) was used where the pentacene and phenylene units had been rotated to the respective conformer and the whole molecule had been symmetrized to at least C2 symmetry.

Results and Discussion

3. Space filling models, crystal structures and calculated lowest energy conformations.

3.1. Space filling models

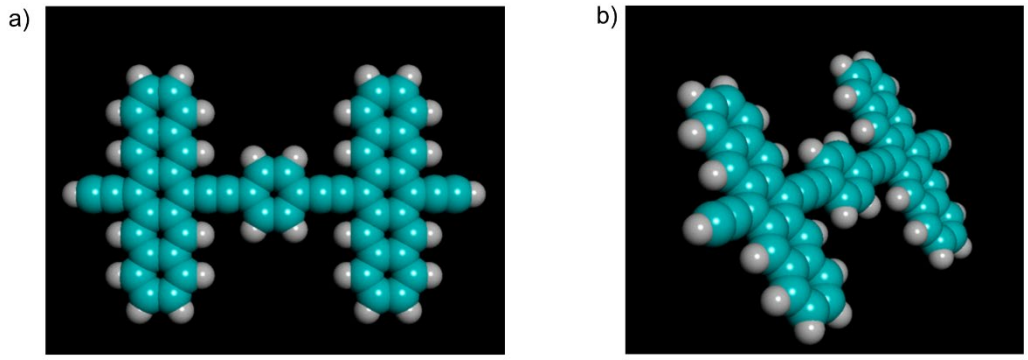

Figure S3.1. Space filling model of the global minimum of **PD1** from Figure 1b with top view (a) and front view (b).

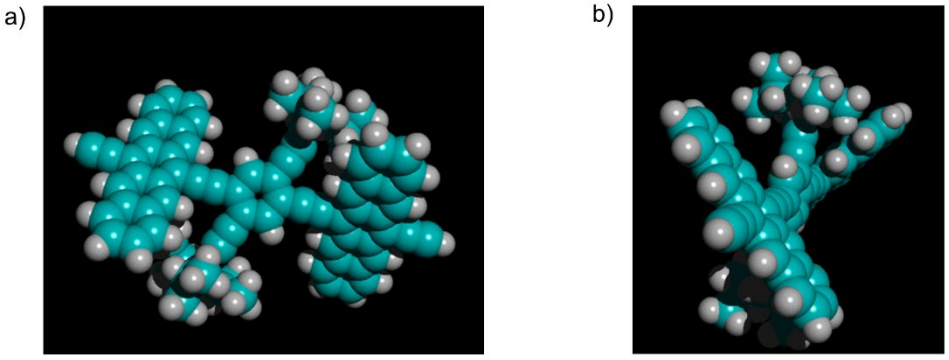

Figure S3.2. Space filling model of the global minimum of **PD2** from Figure 1b with top view (a) and front view (b).

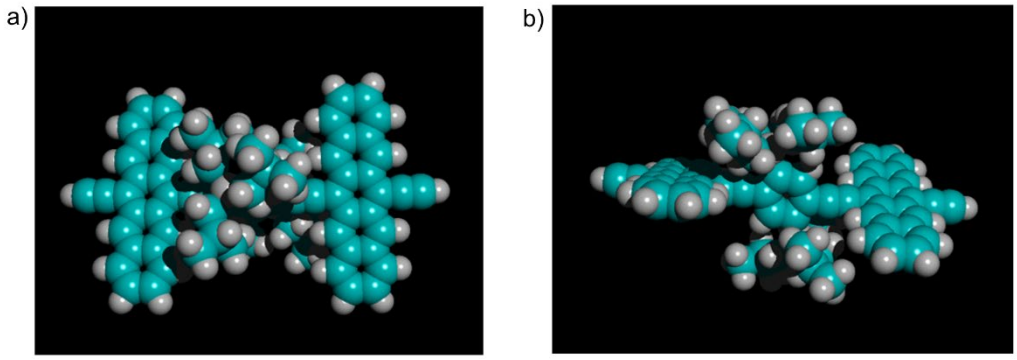

Figure S3.3. Space filling model of the global minimum of **PD3** from Figure 1b with top view (a) and side view (b).

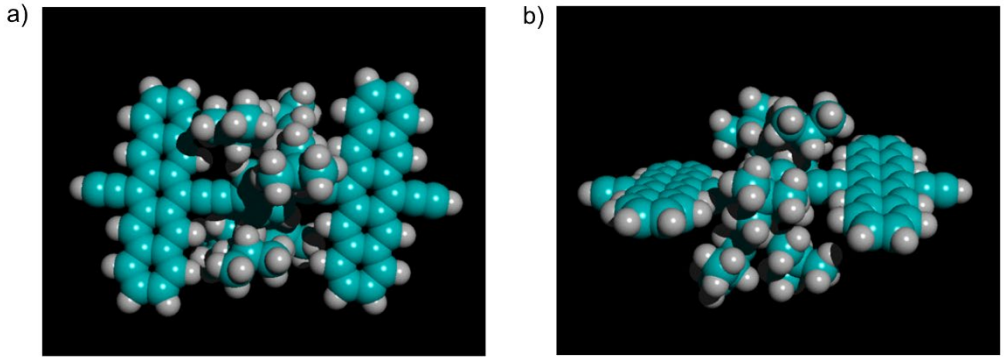

Figure S3.4. Space filling model of the local minimum of **PD3** from Figure S3.8 with top view (a) and side view (b).

3.2. Crystal structures of **PD1-3.**

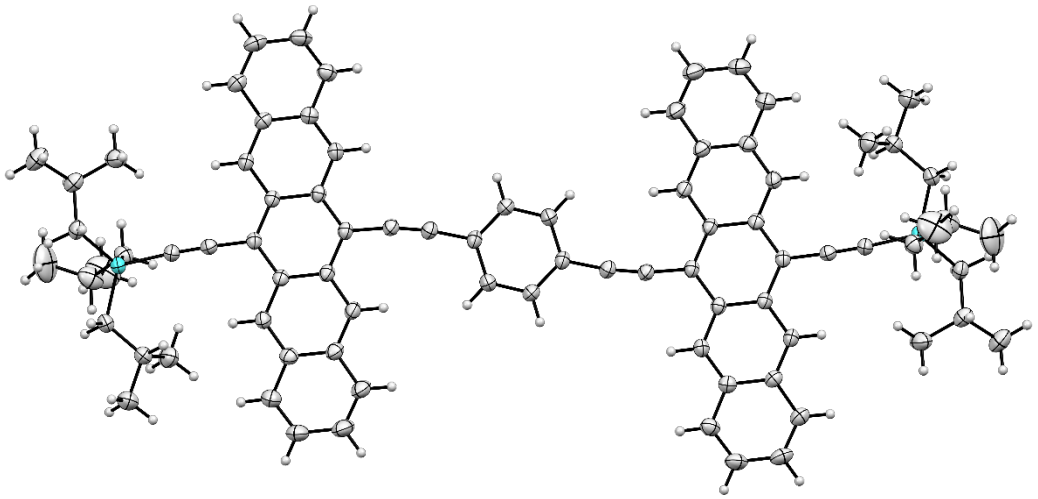

Figure S3.5. Crystal structure of **PD1**. The pentacene units and phenylene-bridge units are coplanar. Non-hydrogen atoms are represented by Gaussian ellipsoids at the 30% probability level.

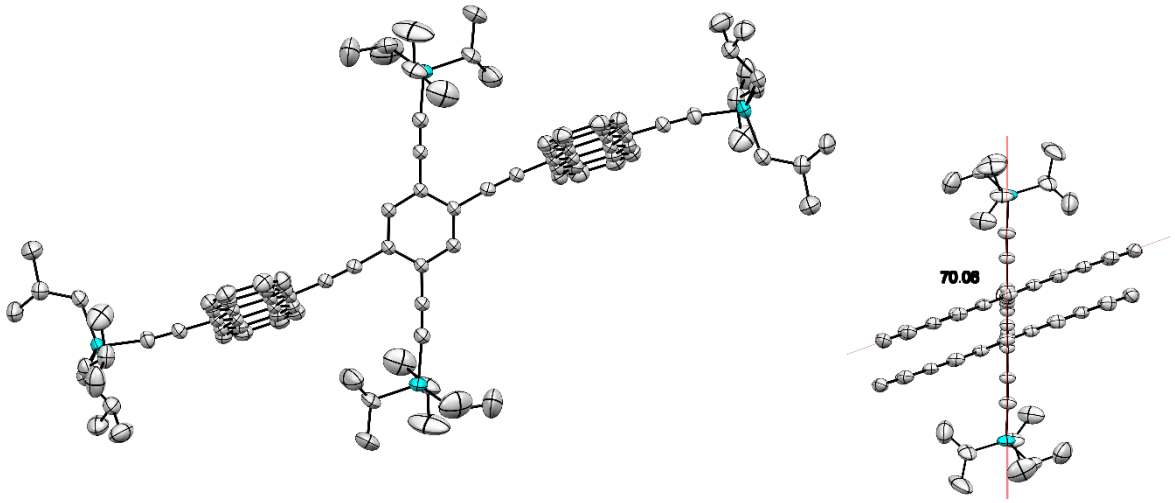

Figure S3.6. Crystal structure of **PD2**. The pentacene units are staggered coplanar in the sense that they lie off-axis across the central phenylene-ring, however, they share a common plane and form a 70.1° angle to the phenylene-bridge unit. Non-hydrogen atoms are represented by Gaussian ellipsoids at the 30% probability level. Hydrogen atoms were omitted for clarity. Right: triisobutylsilyl groups along the long axis of the compound were removed for clarity.

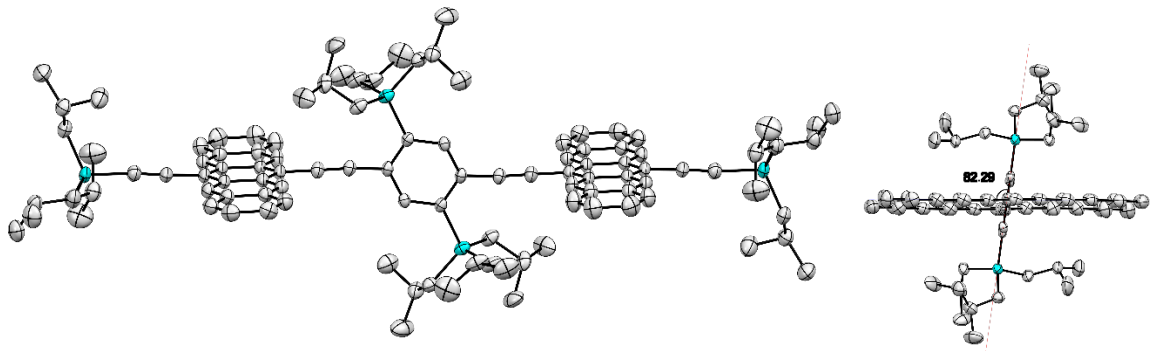

Figure S3.7. Crystal structure of **PD3**. The pentacene units are staggered coplanar in the sense that they lie off-axis across the central phenylene-ring, however, they share a common plane and form an 82.3° angle to the phenylene-bridge unit. Non-hydrogen atoms are represented by Gaussian ellipsoids at the 30% probability level. Hydrogen atoms were omitted for clarity. Right: triisobutylsilyl groups along the long axis of the compound were removed for clarity.

3.3. Local energy minimum conformer of **PD3.**

Figure S3.8 shows a local energy minimum conformation of **PD3** that has been identified in addition to the conformers obtained in the dihedral scan in Figure 1. This structure was calculated in an unrestricted energy optimization, starting with the geometry of the local minimum of the dihedral scan (Figure 1a). The total energy of this conformer is 7.76 meV above the energy of the global minimum conformation. Because this conformer is non-symmetrical, with a slightly bent phenylene bridge, the dihedral angle between the phenylene bridge and one of the pentacene units is not uniquely defined but depends on which of the four possible combinations of the four atoms defining the dihedral angle that are used (Figure S2.1). The four values of the dihedral angle between the phenylene bridge and one of the pentacene units are thus 22.2°, 25.8°, 36.0° and 38.1°.

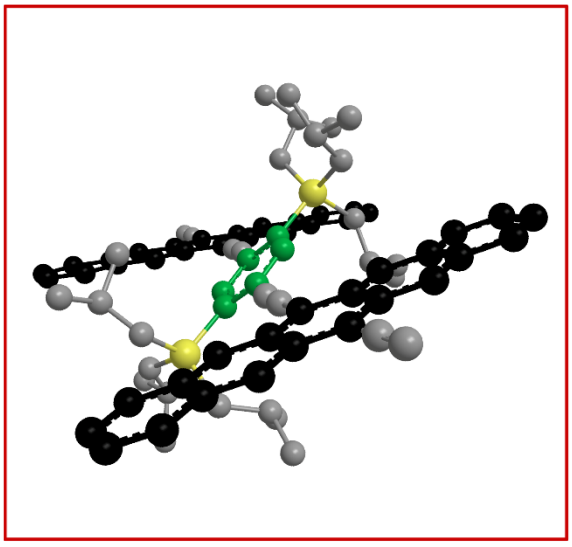

Figure S3.8. A local minimum of **PD3** in addition to the conformers obtained in the dihedral scan in Figure 1. Calculated using DFT, B3LYP, 6-31G(dp).

4. Triplet sensitization of PD1–3

Figure S4.1 A–C present nsTA spectra from the triplet sensitization experiments of **PD1**, **PD2,** and **PD3** with platinum octaethylporphyrin (**PtOEP**) as sensitizer. In Figure S4.1 D–F, the sensitized triplet spectra at long time delays are compared with the corresponding triplet pair evolution associated spectra (EAS) obtained from global analysis of the fsTA data. The sensitized triplet (T_0T_1) is, for all dimers, marginally red shifted relative to the triplet pair EAS. Furthermore, the sensitized spectra of mainly **PD1** and **PD3**, but to a smaller degree also **PD2**, have narrower bands than the triplet pairs generated from SF. The electronic interactions between the triplet states of the strongly correlated triplet pair on a single dimer compared to a single independent triplet state in the case of the sensitization is the main reason for these spectral discrepancies. There are no discernible spectral changes of the triplet pair spectra for any of the dimers during its lifetime indicating that the short lifetime of <200 ps is not sufficiently long to allow for decorrelation of the triplet pair. A second potential reason for the broadened spectra could be that there is a distribution of triplet pair states with varying degree of coupling for the different conformers that are being populated simultaneously. Another difference can be found on the low energy side of the ground state bleach at around 700 nm where the triplet pair have an absorptive feature that is absent for the sensitized triplet. This band, which decays at roughly the same rate as the 500 nm band, is further indication that the triplets are not decorrelated at any point in the room temperature measurements. This band has previously been attributed to triplet pair absorption in several experimental studies of pentacene dimers,[9, 10] and theoretical work has also investigated and confirmed major spectroscopic differences between the strongly correlated triplet pair and isolated triplet states.[11]

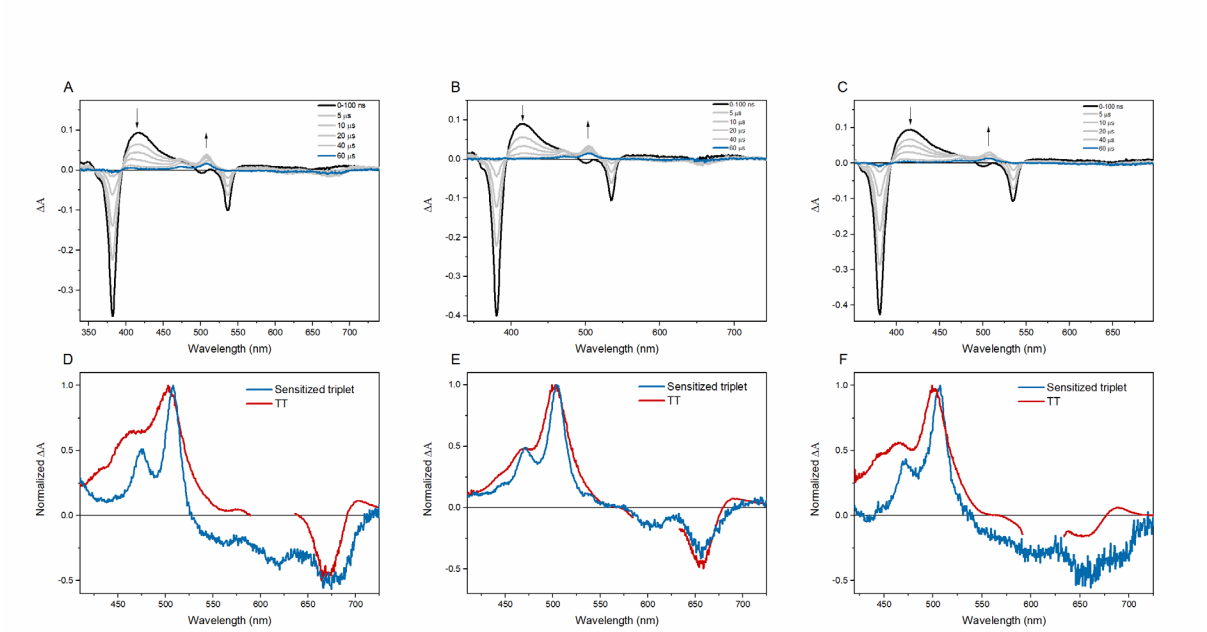

Figure S4.1. Triplet sensitization. (A–C) shows the nsTA spectra with a pump pulse at 536 nm in toluene exciting primarily platinum octaethylporphyrin (**PtOEP**, 17 µM) followed by triplet energy transfer to **PD1** (80 µM), **PD2** (81 µM), and **PD3** (83 µM) in A, B, and C, respectively. (D–F) shows the triplet pair EAS in toluene obtained from global analysis together with the sensitized triplet spectra at long time delays where most of the residual **PtOEP** triplet signal has decayed.

5. Pentacene-pentacene superexchange electronic coupling

The substituents on the phenylene linker in **PD1–3** affect the energetics of the phenylene moiety that connects the pentacene units. This could give rise to varying degree of superexchange electronic coupling between the pentacene units for the three pentacene dimers because the energetics of the linker determines the tunneling barrier of superexchange electronic coupling.[12] In order to exclude this effect as the cause of the different rates of SF observed for the pentacene dimers, the energetics of the phenylene linkers were investigated by computational chemistry. The calculated lowest energy singlet transitions of the linkers can be seen in Figure S5.1. The linker singlet excited state is approximately 3, 2.2 and 2.8 eV higher than the singlet excited state of the corresponding pentacene dimers **PD1**, **PD2,** and **PD3** respectively. Based on this computational result it would be expected that **PD2** should show the strongest pentacene-pentacene electronic coupling and thereby the most redshifted absorption onset and highest rate of SF. However, this is contradicted by experimental observations, Figure 3 and 4. The lack of a trend correlating the energetics of the phenylene linker with the absorption onset and rate of SF shows that the varying degree of pentacene-pentacene superexchange electronic coupling caused by the silyl substituents cannot explain the observed rates of SF for **PD1–3**. The computational results discussed here corroborate well with the experimental UV-Vis spectra of the linkers presented in Figure S5.2. Although the absorption peaks of experimental data don't exactly match the calculated transitions, the general trend from the calculations is apparent with absorption onsets at roughly 3.6 eV for **PD2**, 3.88 eV for **PD3,** and 4.27 eV for **PD1**.

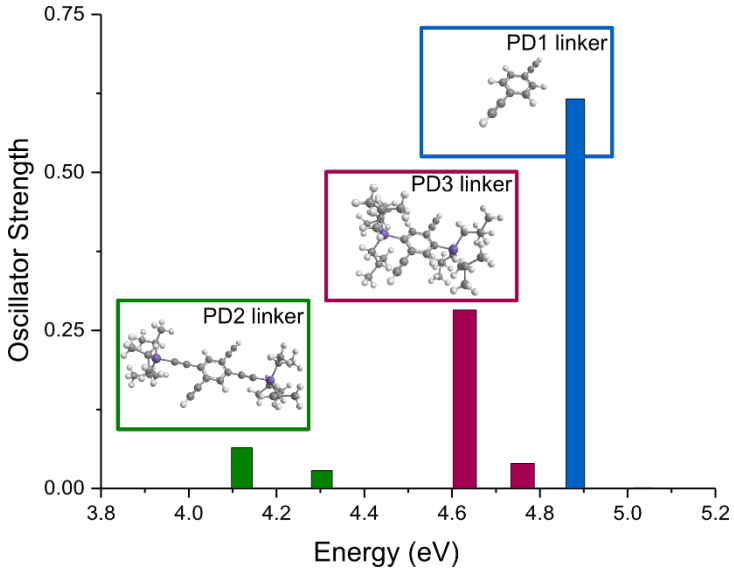

Figure S5.1. Lowest energy single transition of the phenylene linkers connecting the pentacene units in **PD1–3**. The pentacene units in the dimer have here been replaced by hydrogen and the structure has been optimized using DFT (B3LYP, 6-31G(d,p)) . Singlet electronic transitions were then calculated using TDDFT (CAM-B3LYP, 6-31G(d,p)).

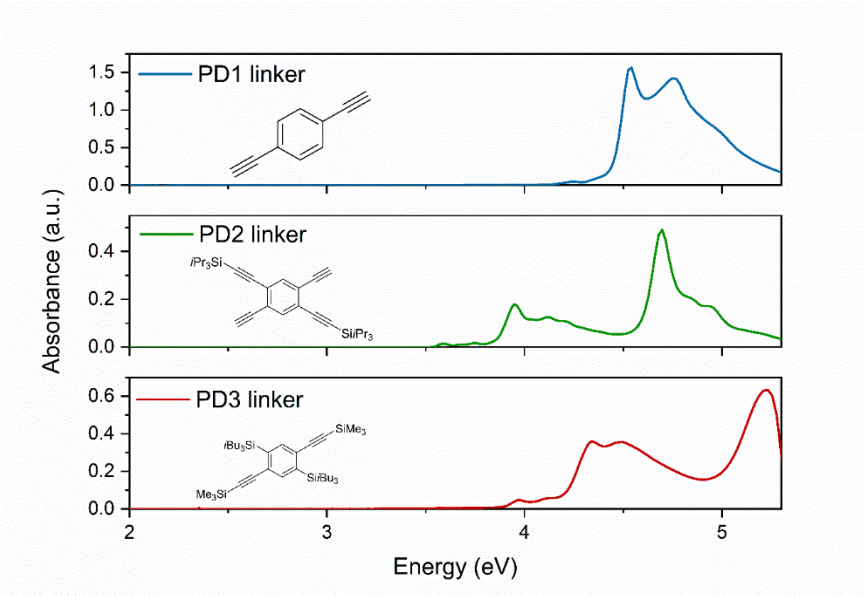

Figure S5.2. Absorption spectra of the bridge units used for **PD1**, **PD2** and **PD3**, respectively. Note that the **PD3** linker is modified with protective groups.

6. Solvent polarity dependence of SF

Figure S6.1 shows the room-temperature fsTA spectra and the corresponding evolution associated spectra (EAS) of the dimers in benzonitrile at room temperature following excitation at 612 nm. Just as for toluene, a two-component sequential model could be fit satisfactorily to the data. The estimated time constants for the benzonitrile measurements shown here are presented in Table S6.1 together with the lifetimes obtained in toluene. For **PD2** and **PD3** there is a clear trend with faster decay of the initial S_0S_1 in the more polar solvent, indicating faster and more efficient SF. However, for **PD1** the lifetime appears to be longer in benzonitrile. The reason for this is likely that the S_0S_1 decays within our instrument response function. Evidence that this is the case can be seen in the EAS of **PD1** in Figure S6.1b. Here, the S_0S_1 has much more triplet character than the corresponding component in toluene indicating that the S_1S_0 is under-resolved in benzonitrile and the first component is here not the pure S_0S_1. For **PD1** in Figure S6.1a we note that there is a small amount of impurity or possibly degradation product with absorption around 460 nm that persists for several hundred ps that is only observed in benzonitrile. The signal from the impurity was too small to be accurately modeled and was not deemed necessary to be included in the fitting.

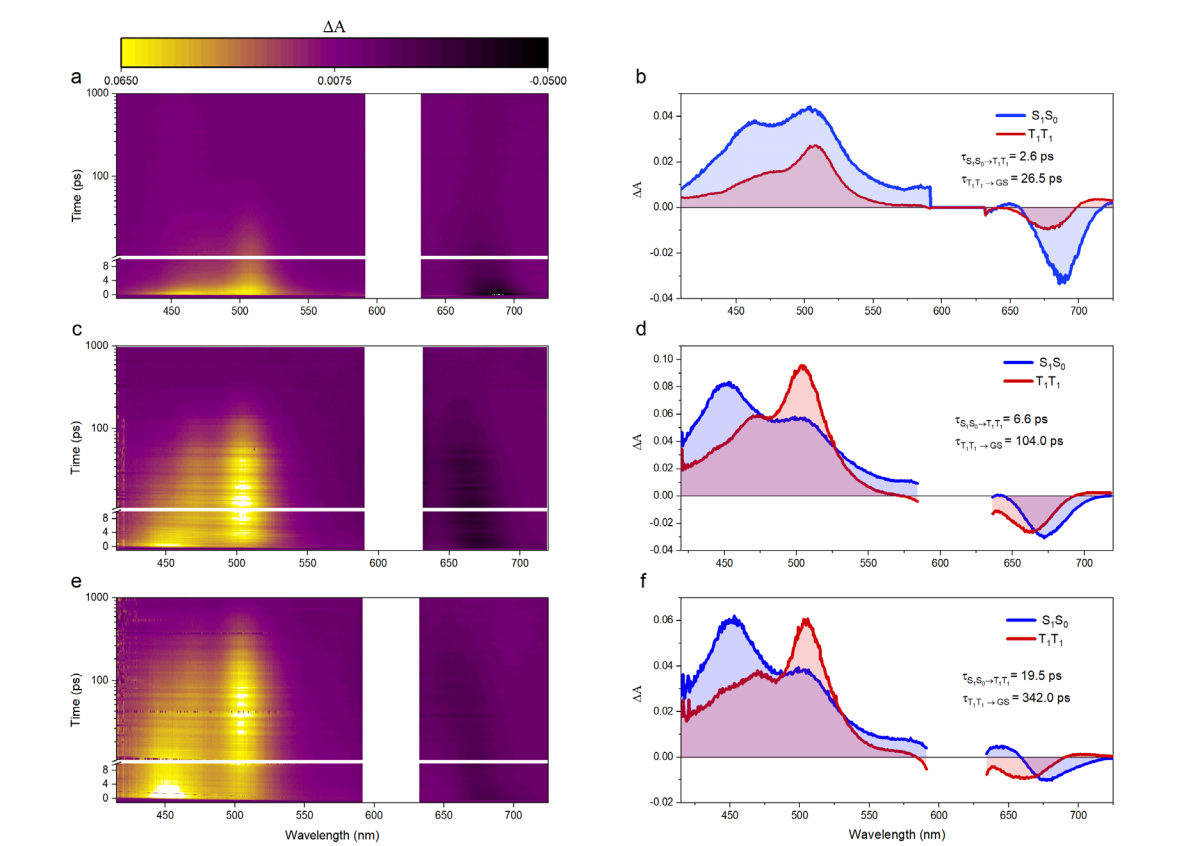

Figure S6.1. Room temperature transient absorption spectra and corresponding evolution associated decay spectra of dimers **PD1** (a,b), **PD2** (c,d), and **PD3** (e,f). All three dimers were fit to a two-component sequential model using global analysis with components and lifetimes indicated in the figure. The measurements were performed in benzonitrile with a pump pulse at 612 nm. The pump scatter near the excitation wavelength has been removed for clarity.

Table S6.1. fsTA time constants from global analysis of **PD1**, **PD2**, and **PD3** in toluene and benzonitrile with a pump pulse at 612 nm.

	PD1 toluene	**PD1** benzonitrile	**PD2** toluene	**PD2** benzonitrile	**PD3** toluene	**PD3** benzonitrile
$\tau_{S0S1\rightarrow T1T1}$ (ps)	1.3	2.6	12.7	6.6	24.3	19.5
$\tau_{T1T1\rightarrow GS}$ (ps)	13.0	26.5	94.1	104.0	199.0	342.0

7. Rotational conformation population distribution

The potential energy of rotation shown in Figure 1a can be used to calculate the distribution of conformers that are present at different temperatures. The probability distribution, P (θ, T), for the conformations with different pentacene-phenylene dihedral angle, θ, at temperature, T, is given from the Boltzmann distribution

$$P(\theta, T) = \frac{e^{\frac{-E(\theta)}{k_B T}}}{\int e^{\frac{-E(\theta)}{k_B T}} dT}$$

where $E(\theta)$ is the potential energy of rotation from DFT calculations. The calculated probability distribution for **PD1–3** at 100 K and 300 K can be seen in Figure S7.1. At room temperature, the full range of rotational conformers of **PD1** and **PD2** are present, but of course with a larger weight on the lower energy conformers. For **PD3**, the range of accessible conformers is limited due to the high rotational barrier, as seen in Figure 1a. However, at 100 K the probability distribution is significantly narrower, especially for **PD3** and **PD2** while **PD1** still has a rotational flexibility of ~50 degrees from the lowest energy conformation. Thus, only a limited number of rotational conformers will be present at 100 K.

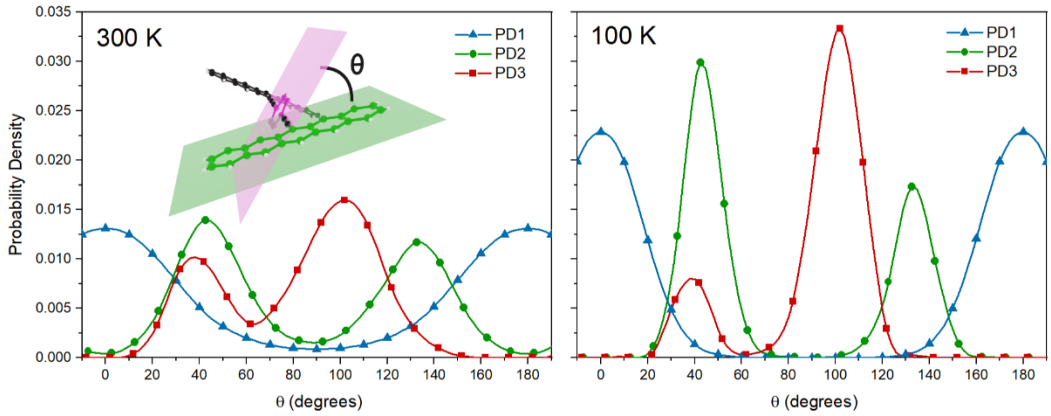

Figure S7.1. Probability distribution function of pentacene dimer rotational conformers at 100 K and 300 K.

8. Room temperature and cryogenic steady state absorption of spectra of PD1–3

Room temperature and cryogenic steady state emission spectra have been measured for **PD1—3** under various conditions in order to exclude formation of aggregates.

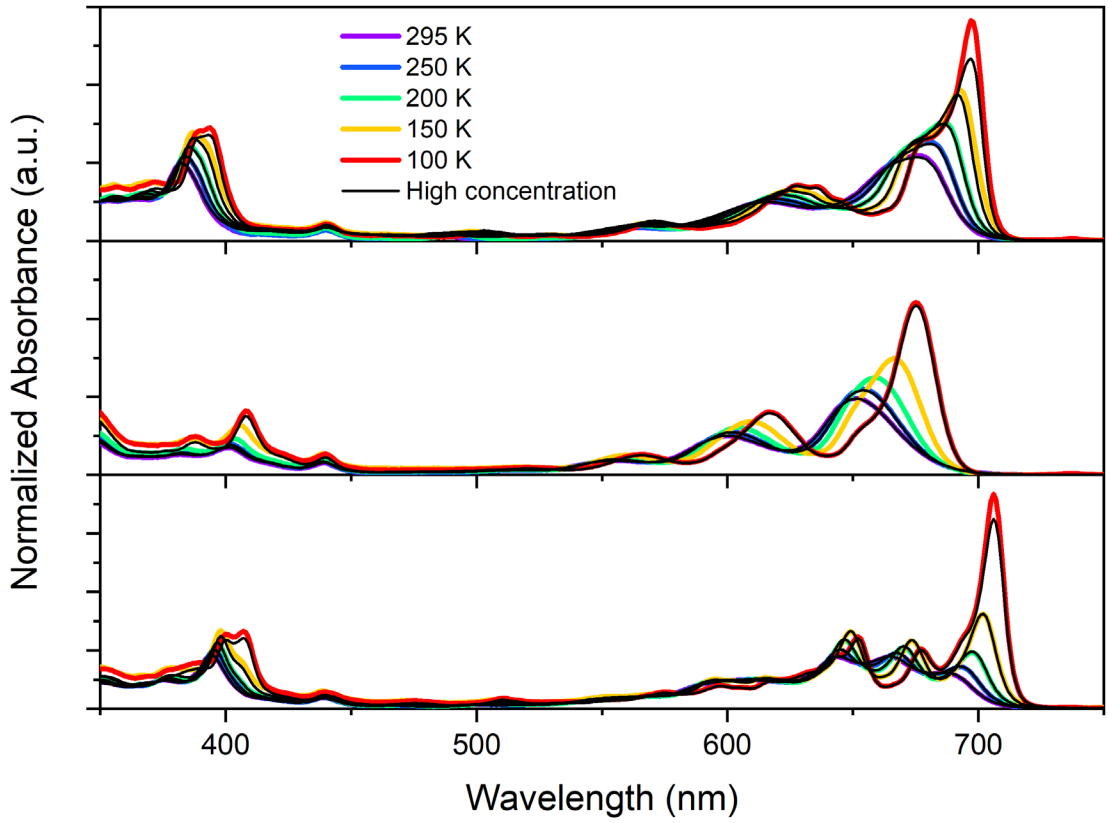

Figure S8.1. Absorption spectra of dimers **PD1** (top), **PD2** (middle), and **PD3** (bottom) in MTHF at temperatures ranging from 295 to 100 K at low (colored) and high concentration (black). The high-concentration spectra have been normalized to the respective low-concentration spectrum at 295 K. The absorption spectra of the high- and low-concentration samples overlap very well in the entire investigated spectral range. Minor deviation is seen at the lowest energy band where the high-concentration absorbance is slightly lower than the corresponding low concentration absorbance at 100 K. This is most likely a consequence of inaccurate temperature control at this temperature. High concentration refers to 90, 111, and 30 μM for **PD1**, **PD2**, and **PD3** respectively. Low concentration is 1.4, 1.7, and 1.3 μM for **PD1**, **PD2**, and **PD3** respectively.

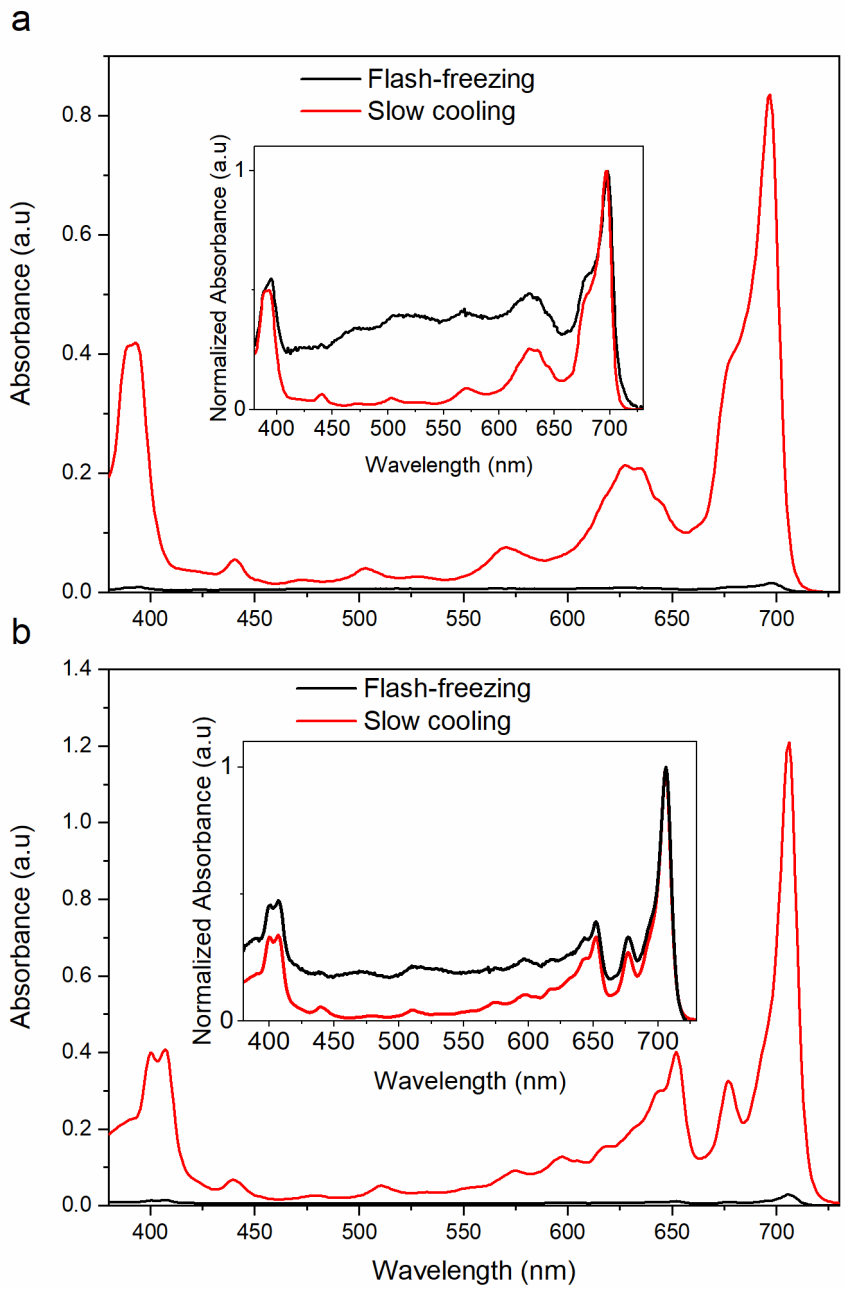

Figure S8.2. Steady state absorption spectra of a) **PD1** and b) **PD3** in MTHF at 100 K. The black trace shows the absorption of a highly dilute sample that was flash-frozen by submerging it in liquid nitrogen previously poured into the cryostat sample holder. The red trace is the absorption of a sample that was slowly cooled from 295 K to 100 K and where equilibrium was allowed to be reached at intervals of 50 K during the cooling process. The inset showing the normalized absorption reveals that both spectra exhibit identical growth of the lowest energy band. It is unlikely that the very low concentration and the extremely rapid glass formation would provide enough time for aggregation to occur and this result is thus a solid indication that the growing band is not a result of aggregation. The different absorption between the two samples at shorter wavelengths is caused by faulty baseline correction as a result of the low concentration as well as scattering.

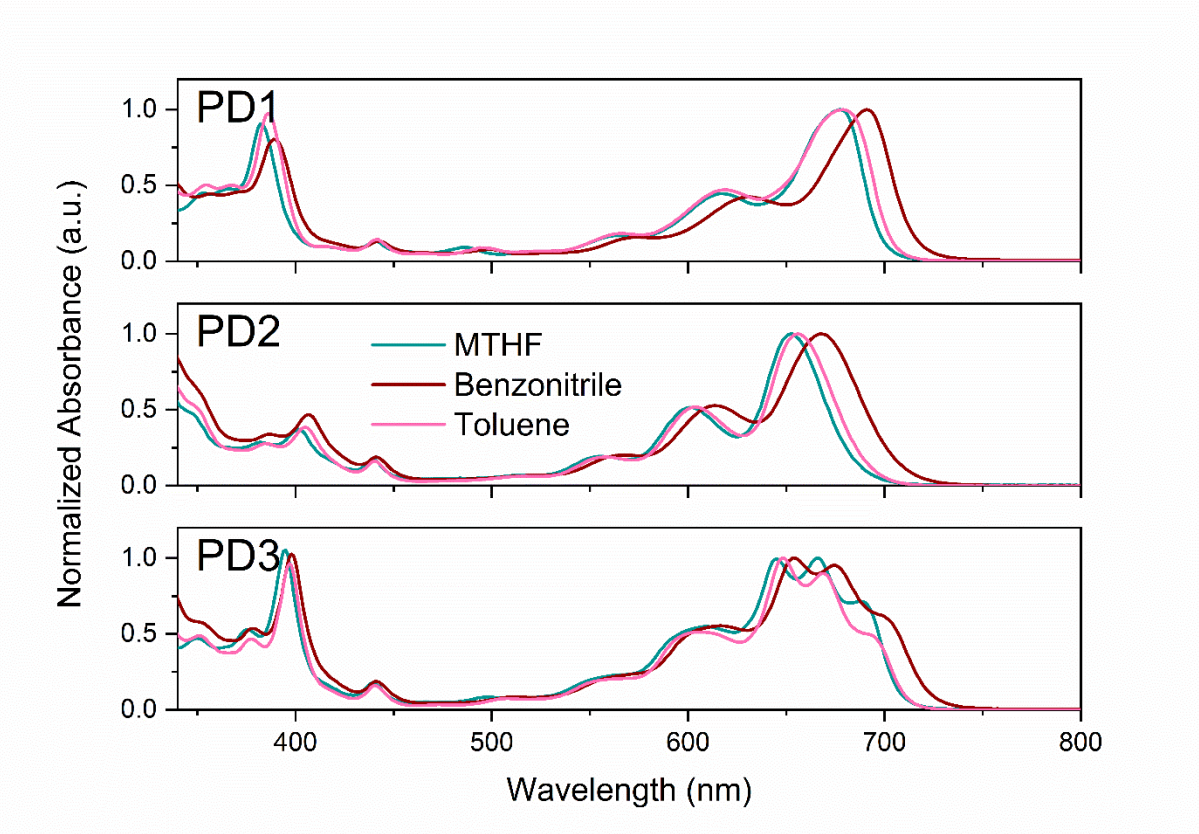

Figure S8.3. Normalized steady state absorption spectra of **PD1–3** in MTHF, benzonitrile, and toluene.

9. Cryogenic measurements of PM

Cryogenic absorption measurements of the monomer, **PM**, reveal that the absorption spectra (Figure S9.1) red shifts and that the amplitude of the lowest energy vibronic transition increases relative to the other absorption bands. Similar features have been reported for pentacene in a matrix isolation absorption spectrum, confirming that this is not caused by molecular aggregation.[13] The growth of the lowest energy band is similar to that observed for the dimers **PD1–3** (Figure 4). We speculate that it originates from the flattening of the single pentacene unit at low temperature. In stark contrast to the dimers, the excited state dynamics of **PM** at 100 K are independent of the excitation wavelength as indicated by the identical fsTA spectra; obtained by exciting the red-most absorption band and at higher excitation energy (Figure S9.2). The room temperature transient absorption spectrum of **PM** is shown for comparison in Figure S9.3. The low temperature and room temperature spectra display similar kinetics, but with slightly different spectral evolution. It appears that the intersystem crossing decay pathway, which at room temperature produces a small amount of triplet population and gives rise to the peak at 500 nm, is suppressed at cryogenic temperatures.

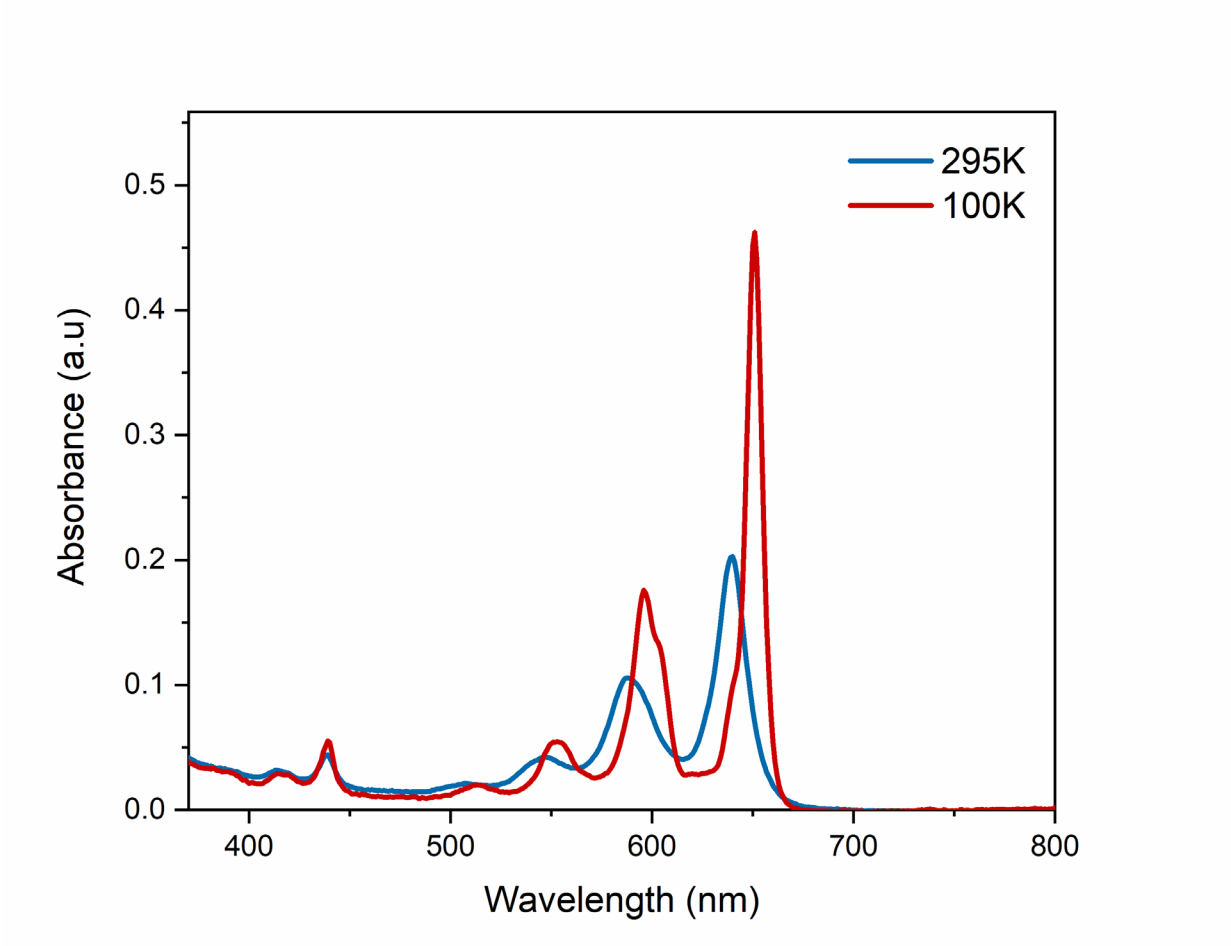

Figure S9.1. Ground state absorption spectra of the monomer, **PM** (25 µM), at 295 and 100 K in MTHF.

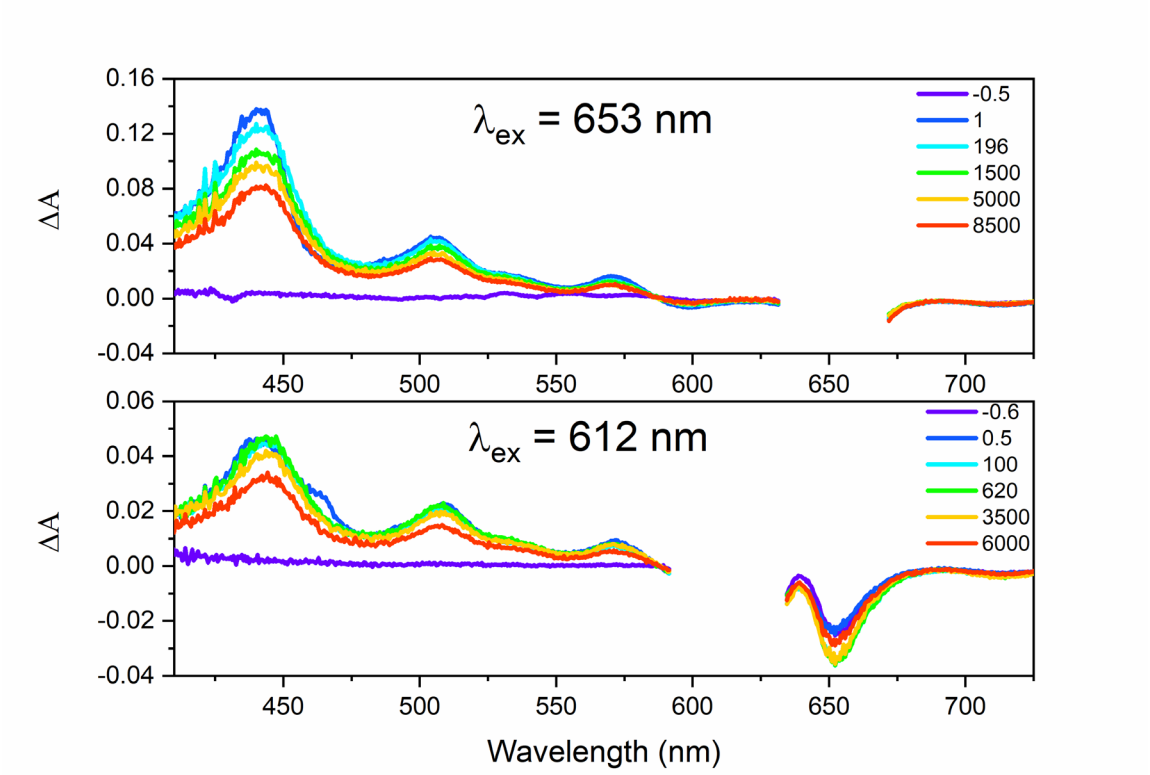

Figure S9.2. Transient absorption spectra of **PM** (90 µM) at 100 K in MTHF with an excitation wavelength of 653 nm (top) and 612 nm (bottom) with time delay in ps. The pump scatter has been removed for clarity.

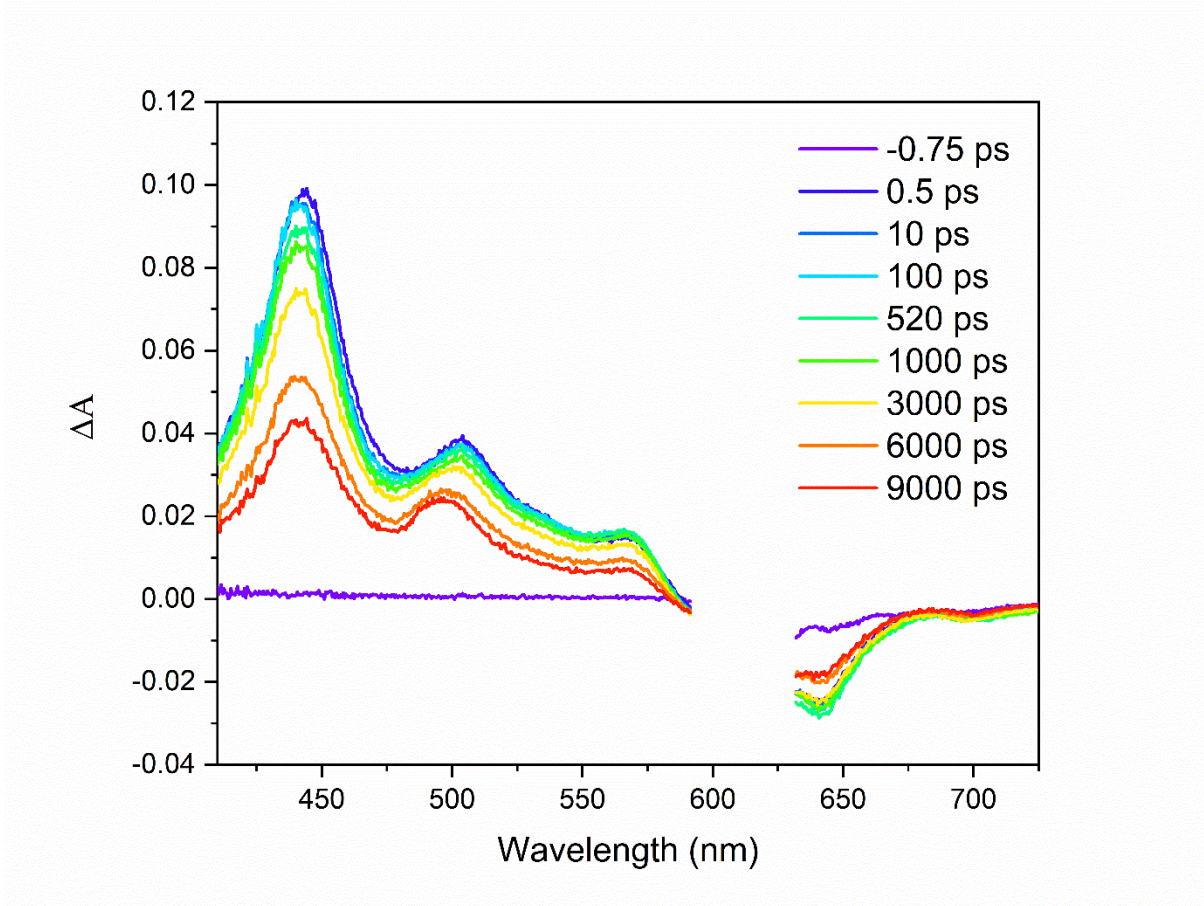

Figure S9.3. Room temperature transient absorption spectra of **PM** (95 µM) at 100 K in toluene with an excitation wavelength of 612 nm. The pump scatter has been removed for clarity.

10. Fluorescence excitation and emission spectra of PD1–3

All three pentacene dimers are slightly emissive with a fluorescence quantum yield around or less than 1%. Hence, the fluorescence of the pentacene dimers is heavily quenched in comparison to a corresponding pentacene monomer, **PM**, which has a fluorescence quantum yield of approximately 75%. Making quantitative conclusions based on the very low fluorescence intensity from the pentacene dimers is difficult because any minor impurity of a highly fluorescent pentacene derivative will influence the results. However, the excitation spectrum can still be used for qualitative discussions. The excitation spectrum of the pentacene dimers is similar but does not overlap exactly with the absorption spectrum of the respective compound, see Figure S10.1. It should be noted that the excitation spectrum is blue shifted compared to the absorption spectrum for the lowest energy vibrational bands for all pentacene dimers. Further, the absorption shoulder at ~695 nm for **PD3** is absent in the excitation spectrum while the other two **PD3**-characteristic peaks at 648 and 668 nm are clearly present. The intensity difference between the absorption and excitation spectra in the blue region (λ < 500 nm) is attributed to a minor impurity with a high fluorescence quantum yield. Absence of an excitation band means that the corresponding excited species is non-emissive. Hence, the mismatch between the absorption and excitation spectrum indicates that the absorption bands are composed of multiple transitions, of which some leads to non-emissive excited species and some to more emissive. If the red-most transition in each absorption band corresponds to excitation of a non-emissive species, it will result in an apparent blue shift of the excitation spectrum.

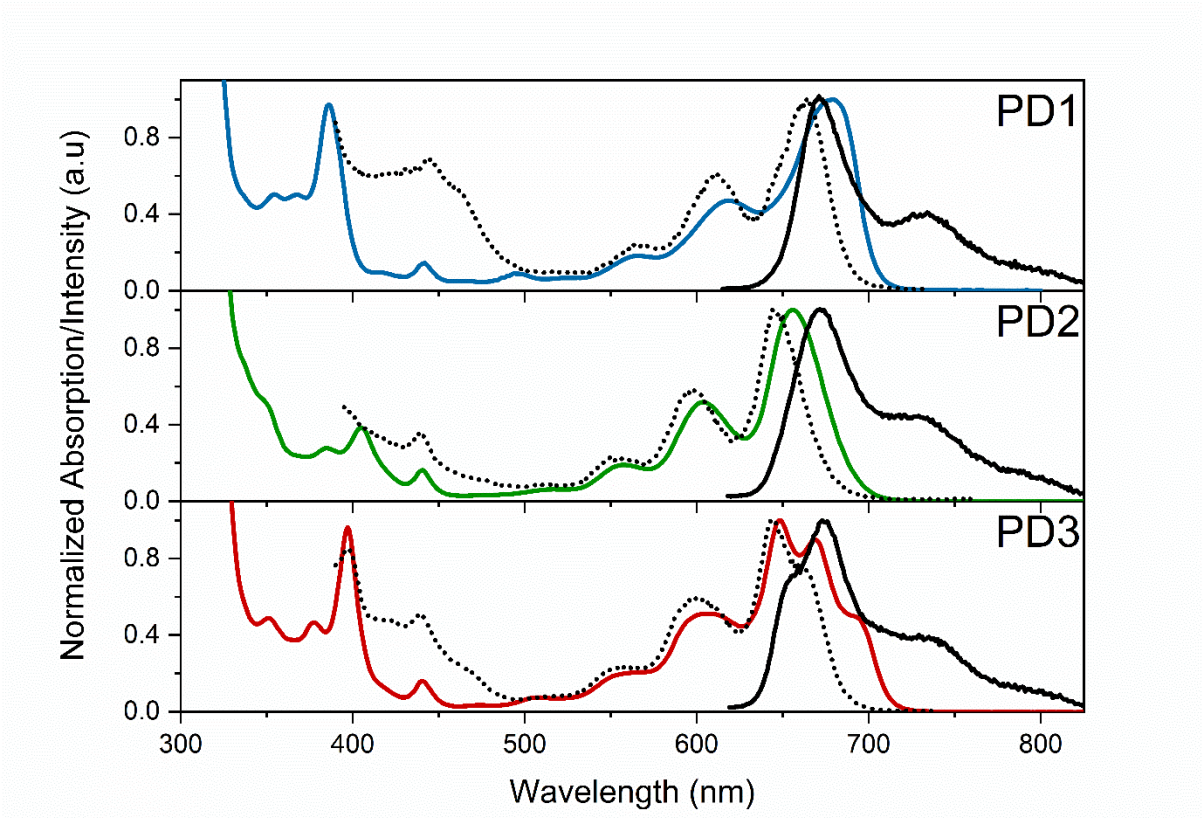

Figure S10.1. Normalized absorption (colored solid lines), fluorescence excitation spectra (dotted lines) and emission spectra (solid black lines) of **PD1–3** in toluene. The fluorescence measurements were performed with an absorbance less than 0.05 for all compounds to ensure minimal inner filter effects.

11. Excitation energy dependent fsTA at 100 K

The full details of the fittings of the triplet excited state kinetics probed at 505 nm as presented in Figure 5 can be found in Table S11.1. The kinetics were fit to a sum of exponentials with the equation shown below.

$$y = y_0 + \sum A_i e^{-x/t_i}$$

We note that **PD3** with an excitation energy of 675 nm displays a slight growth of the triplet excited state signal in the first ps of the measurement as seen in Figure 5. This may very well be triplet formation as a result of SF by another strongly coupled conformer and further highlights the complicated kinetics observed here. This minute growth was not included in the exponential fitting presented here.

Figure S11.1, S11.6 and S11.10 show the fsTA spectra and a few selected single wavelength kinetics of the excitation wavelength dependent fsTA measurements for **PD1**, **PD2** and **PD3**, respectively.

Table S11.1. fsTA time constants from tail-fits of normalized **PD1**, **PD2**, and **PD3** triplet-pair formation and decay at 505 nm at 100 K in MTHF. The final row shows the amplitude weighted average lifetime. Negative amplitudes correspond to a rise in the kinetics.

		PD1			**PD2**			**PD3**	
Excitation wavelength (nm)	628	676	697	614	652	677	651	675	707
y_0	0.03	0.04	0.017	0.05	0	0.03	0	0	–0.003
A_1	0.67	–0.29	1.16	–0.54	–0.35	–0.43	0.51	0.21	1.22
A_2	0.24	0.67	-	0.71	0.48	0.82	–0.34	–0.49	-
A_3	0.15	0.3	-	0.31	0.51	0.22	0.88	1.06	-
τ_1 (ps)	5.4	0.7	3.1	5.8	12.6	4.2	1.6	3.5	1.8
τ_2 (ps)	69	55	-	155	798	147	153	133	-
τ_3 (ps)	1060	1000	-	3300	11480	3230	20900	7380	-
$\tau_{average}$ (ps)	166[a]	350[b]	-	1100[c]	6350[d]	800[e]	-	-	-

[a] Amplitude average of lifetimes τ_1, τ_2, and τ_3. [b] Amplitude average of lifetimes τ_2 and τ_3. [c] Amplitude average of lifetimes τ_2 and τ_3. [d] Amplitude average of lifetimes τ_2 and τ_3. [e] Amplitude average of lifetimes τ_2 and τ_3.

11.1. Global analysis

The single wavelength kinetics presented in Table S11.1 serve well for a qualitative assessment of the triplet kinetics. However, since the singlet excited state also absorbs at 505 nm global analysis was performed on the 100 K fsTA datasets for all three dimers. Slightly different models for each excitation wavelength and dimer must be employed to model the data accurately. It should be emphasized that the models presented here represent only one possibility out of many that can accurately describe the systems' kinetics. A more detailed description of each model is presented in conjunction with the introduction of the model in question.

11.2. Global analysis of PD1

PD1 requires a total of four components to accurately fit the raw data presented in Figure S11.1 for the excitation wavelengths of 628 and 676 nm which preferentially populates the more weakly coupled conformers. The model for these excitation wavelengths is presented in Figure S11.3 and the obtained SAS and population dynamics are presented in Figure S11.2. It is not possible with the current information to properly assign the three final components with very similar SAS (all closely resembling the triplet spectra from the sensitized triplet measurements in Section 4) to any particular spin state or extent of coupling and decorrelation. We can at this stage only note that all triplet components are necessary to achieve a proper fit with the raw data (see Figure S11.5 for a comparison between raw data and model data). A two-component sequential model (Figure S11.4) was used for the data with an excitation wavelength of 697 nm which populates the strongly coupled conformer that fully decays within 15 ps. The rate constants are presented in Table S11.2.

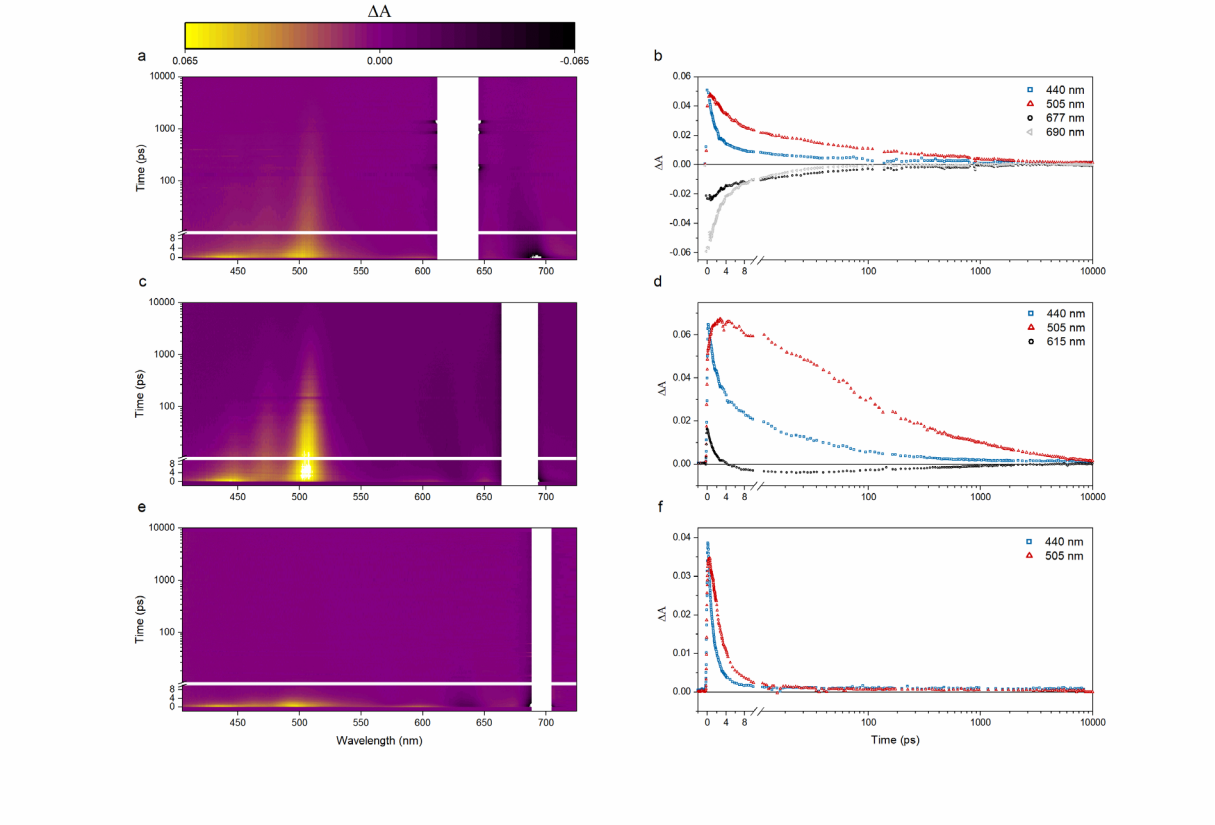

Figure S11.1. Transient absorption spectra and corresponding single wavelength kinetics of **PD1** with an excitation wavelength of 628 nm (a,b), 676 nm (c,d), and 697 nm (e,f). The measurements were performed in MTHF at 100 K. The pump scatter near the excitation wavelength has been removed for clarity.

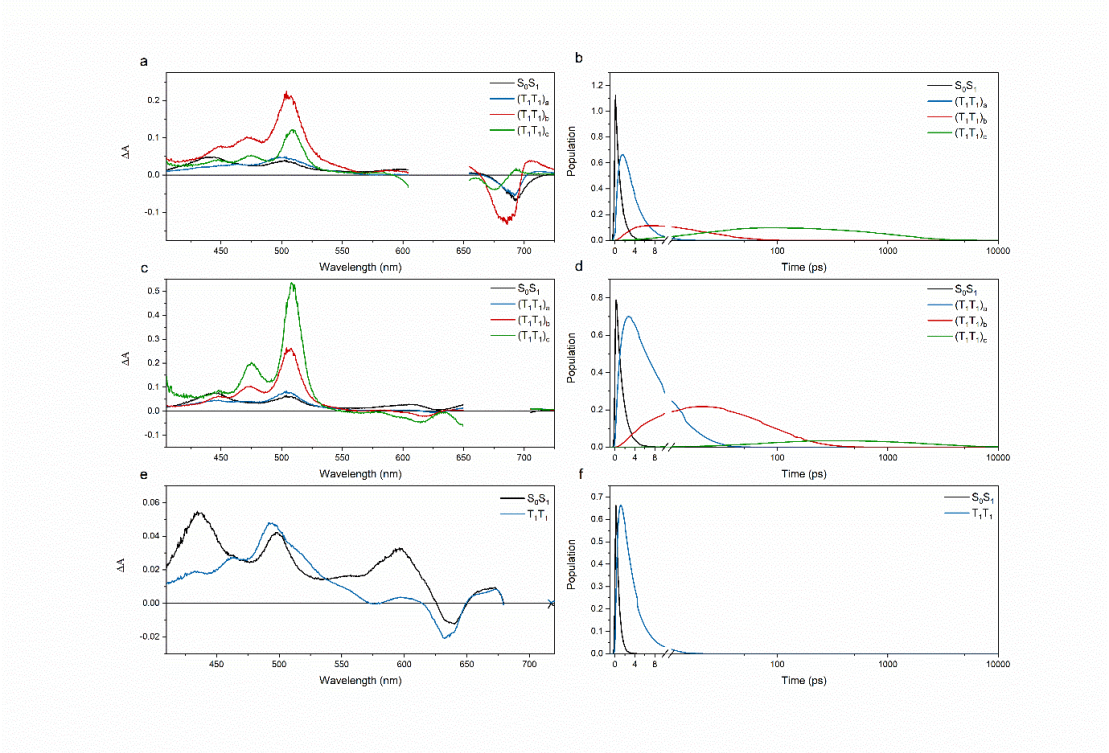

Figure 11.2. SAS and corresponding population dynamics of **PD1** with an excitation wavelength of 628 nm (a,b), 676 nm (c,d), and 697 nm (e,f) for the data in Figure S11.1 using the model in Figure 11.3 for excitation wavelengths 628 and 676 nm and the model in Figure S11.4 for 697 nm.

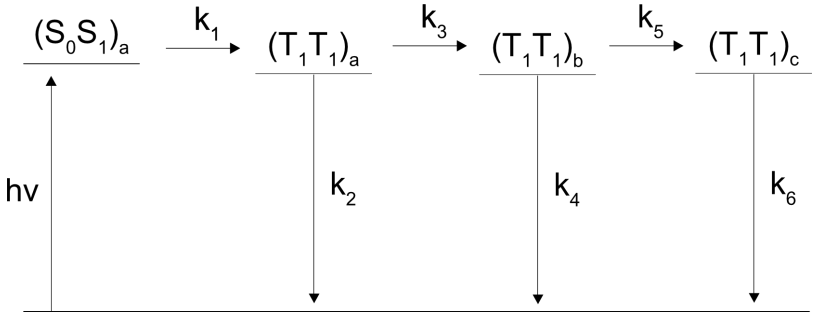

Figure 11.3. Kinetic model used to fit the transient absorption at 100 K data for **PD1** in Figure S11.1 with an excitation wavelength of 628 and 676 nm.

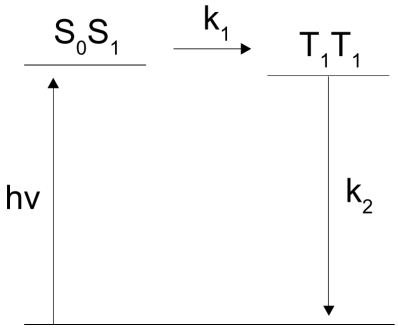

Figure 11.4. Kinetic model used to fit the transient absorption data at 100 K for **PD1** in Figure S11.1 with an excitation wavelength of 697 nm.

Table S11.2. Rate constants for **PD1** at 100 K in MTHF using the kinetic model in Figure S11.3 for excitation wavelengths 628 and 676 nm and Figure S11.4 for 697 nm.

Excitation wavelength (nm)	$1/k_1$ (ps)	$1/k_2$ (ps)	$1/k_3$ (ps)	$1/k_4$ (ps)	$1/k_5$ (ps)	$1/k_6$ (ps)
628	1.0	20	2.7	34.1	82	1300
676	1.3	29	11	680	114	3040
697	0.6	2.8	-	-	-	-

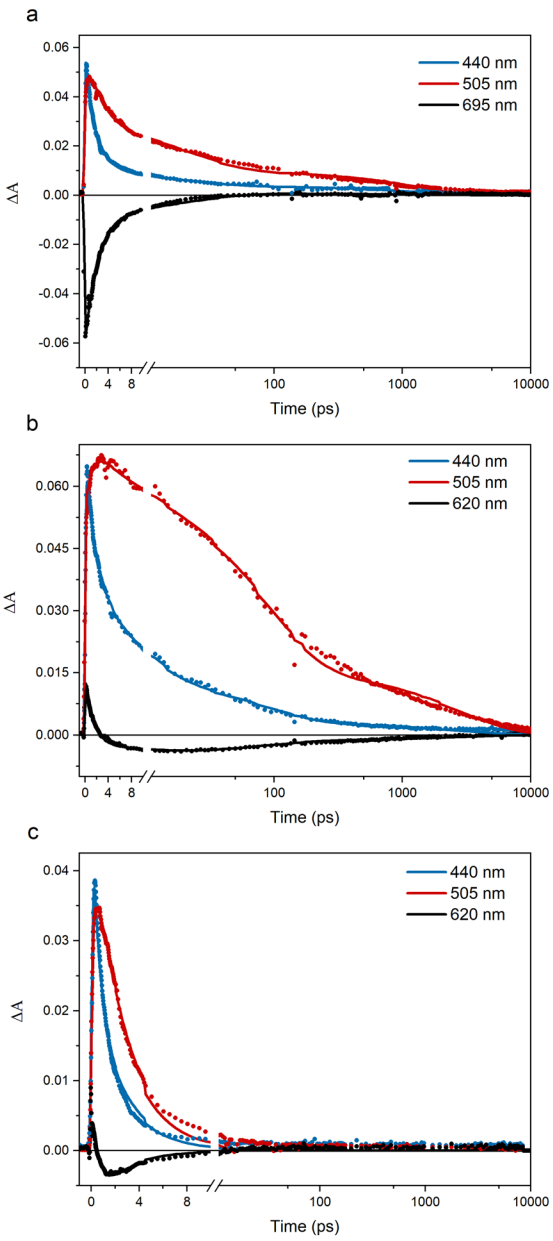

Figure 11.5. Kinetic traces of the fsTA raw data and fittings from the global analysis for a few select wavelengths for **PD1** with an excitation wavelength of (a) 628 nm, (b) 676 nm, and (c) 697 nm.

11.3. Global analysis of PD2

For **PD2**, the fsTA spectra for all three excitation wavelengths in Figure S11.6 could be fit to the model shown in Figure S11.8. The SAS of the third component in Figure S11.7, here denoted T_1+T_1 lacks the absorptive feature around 700 nm which is a distinction of the correlated triplet pair as shown in the comparison with the sensitized triplet spectra in Section 4. This indicates that the triplet specie evolving here could be a more weakly coupled triplet pair or alternatively represent fully independent triplet states. Based on the transient absorption data alone we cannot however conclusively say to what extent the triplet pair has decoupled. The rate constants are presented in Table S11.3 and the quality of the global analysis fitting is shown from a few select single wavelength traces comparing the raw data and model data in Figure S11.9.

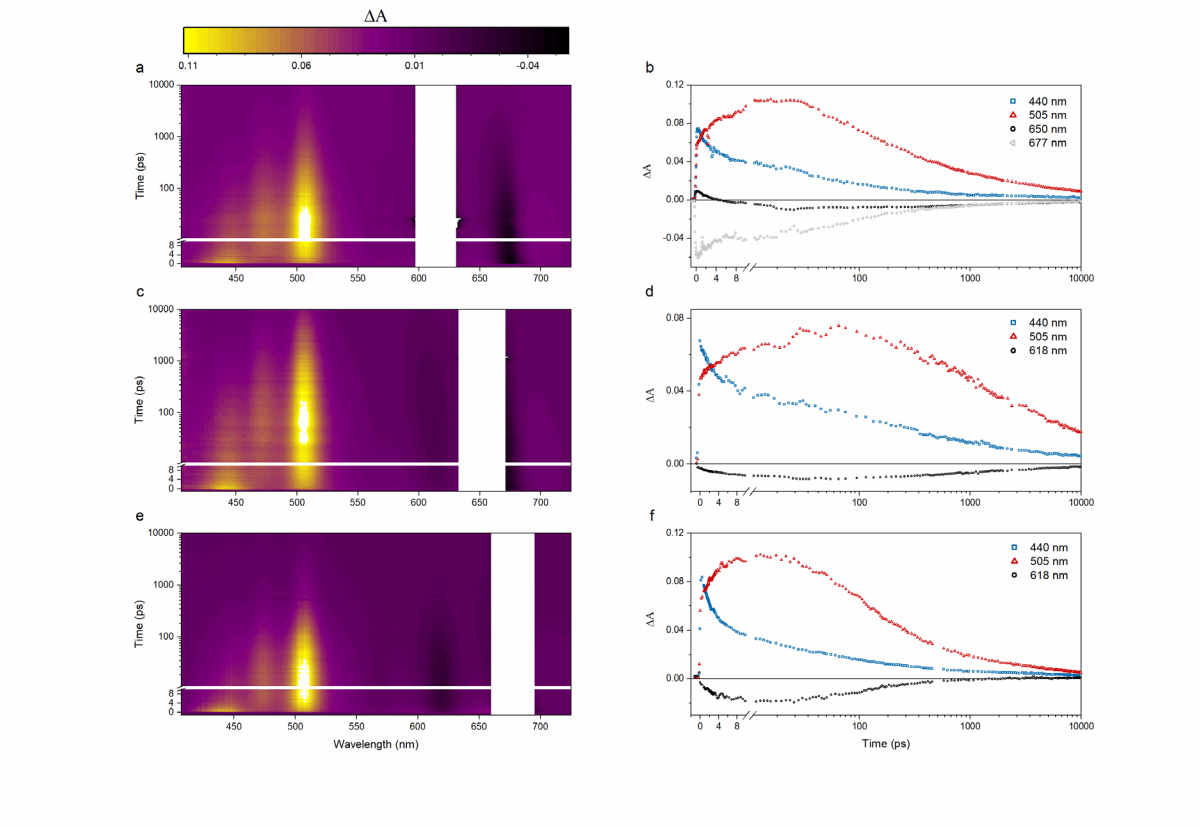

Figure S11.6. Transient absorption spectra and corresponding single wavelength kinetics of **PD2** with an excitation wavelength of 614 nm (a,b), 652 nm (c,d), and 677 nm (e,f). The measurements were performed in MTHF at 100 K. The pump scatter near the excitation wavelength has been removed for clarity.

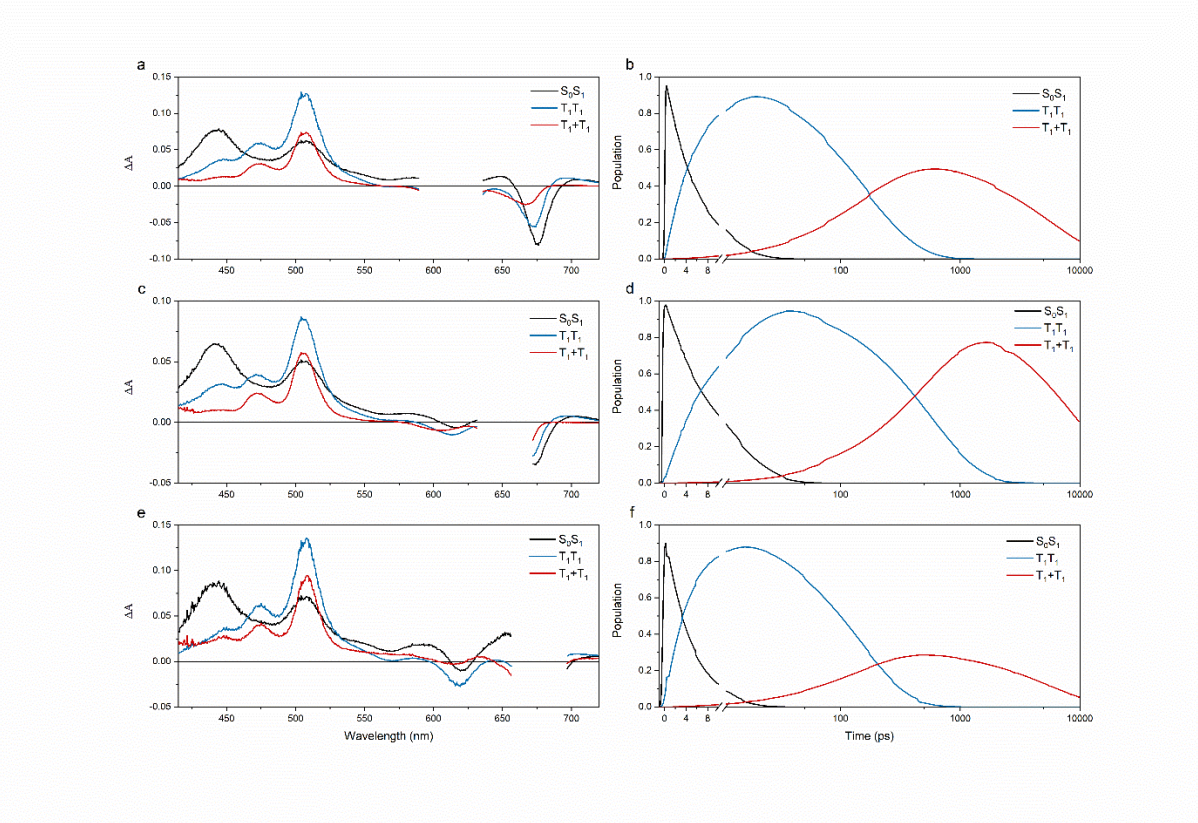

Figure S11.7. SAS and corresponding population dynamics of **PD2** with an excitation wavelength of 614 nm (a,b), 652 nm (c,d), and 677 nm (e,f) for the data in Figure S11.6 using the model in Figure 11.8.

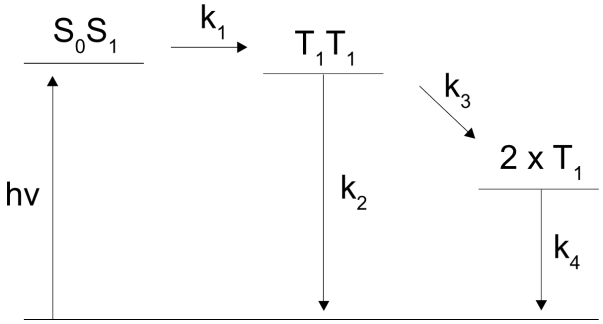

Figure S11.8. Kinetic model used to fit the transient absorption data at 100 K for **PD2** in Figure S11.6 with an excitation wavelength of 614, 652, and 677 nm.

Table S11.3. Rate constants for **PD2** at 100 K in MTHF using the kinetic model in Figure S10.8.

Excitation wavelength (nm)	$1/k_1$ (ps)	$1/k_2$ (ps)	$1/k_3$ (ps)	$1/k_4$ (ps)
614	6.2	385	319	5770
652	10.6	6100	622	9390
677	5.1	213	459	5610

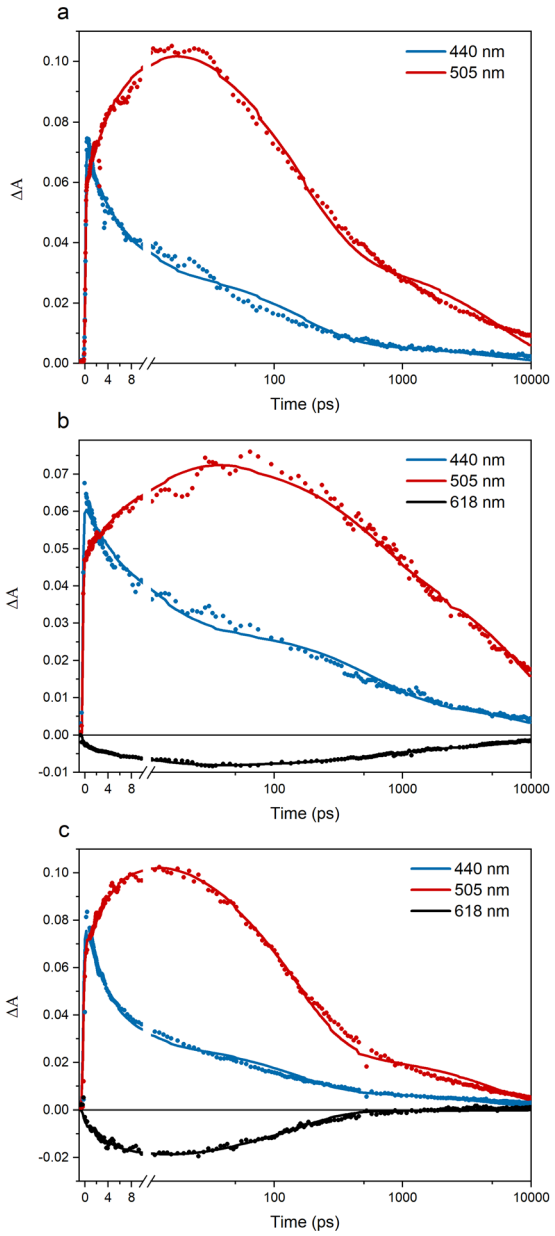

Figure S11.9. Kinetic traces of the raw data and fittings from the global analysis for a few select wavelengths for **PD2** with an excitation wavelength of (a) 614 nm, (b) 652 nm, and (c) 677 nm.

11.4. Global analysis of PD3

The model that was used for the fsTA data of **PD3** with excitation wavelengths of 651 and 675 nm shown in Figure S11.10 is presented in Figure S11.12. This model includes two initial populations where the first component decays very rapidly as seen in Figure S11.11 showing both the SAS and population dynamics. This component is denoted as $(S_0S_1/T_1T_1)_a$ and has mainly triplet character due to the singlet being under-resolved. The fast-decaying component is likely the same strongly coupled conformer that is populated when exciting at 707 nm and it is being populated at higher energies as well due to the expected vibrational progression of the 707 nm band. This conclusion is based on the fact that it decays at a similar rate as the conformer excited selectively at 707 nm (see Table S11.4 for rate constants) in addition to having closely resembling SAS as shown Figure S11.11. Figure S11.14 presents the single wavelength traces where the raw data is plotted together with the modeled data.

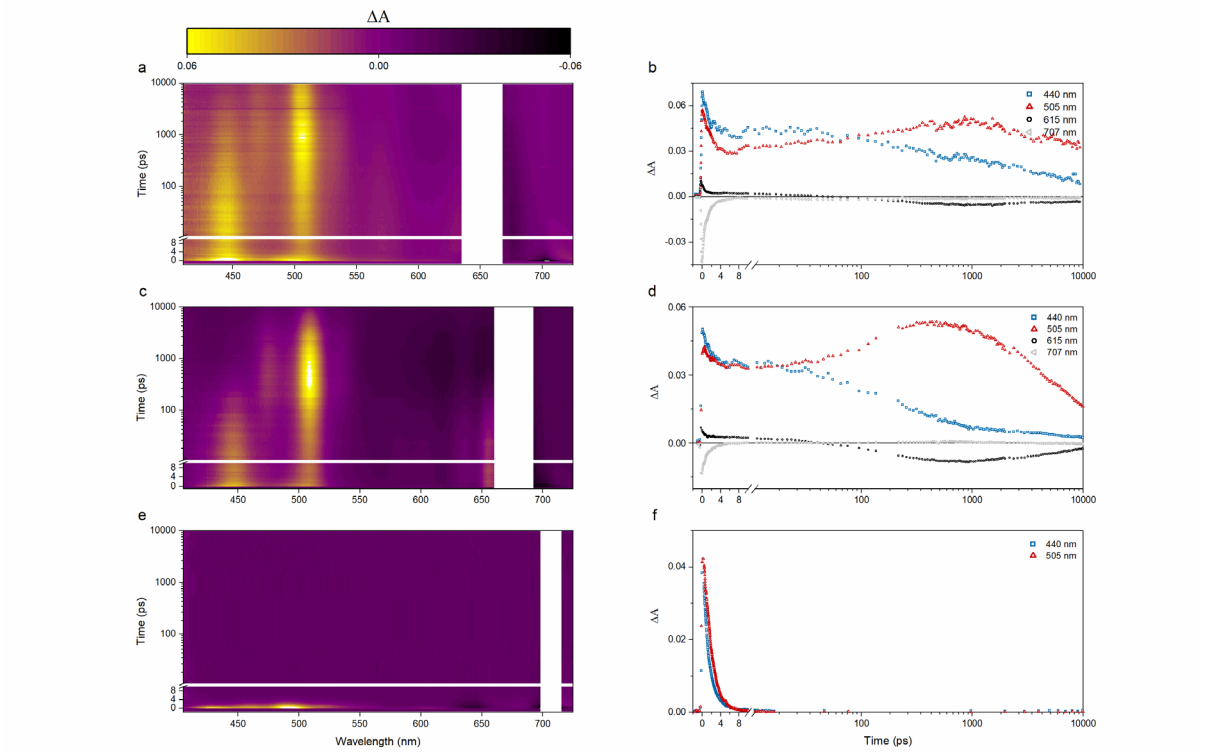

Figure S11.10. Transient absorption spectra and corresponding single wavelength kinetics of **PD3** with an excitation wavelength of 651 nm (a,b), 675 nm (c,d), and 707 nm (e,f). The measurements were performed in MTHF at 100 K. The pump scatter near the excitation wavelength has been removed for clarity.

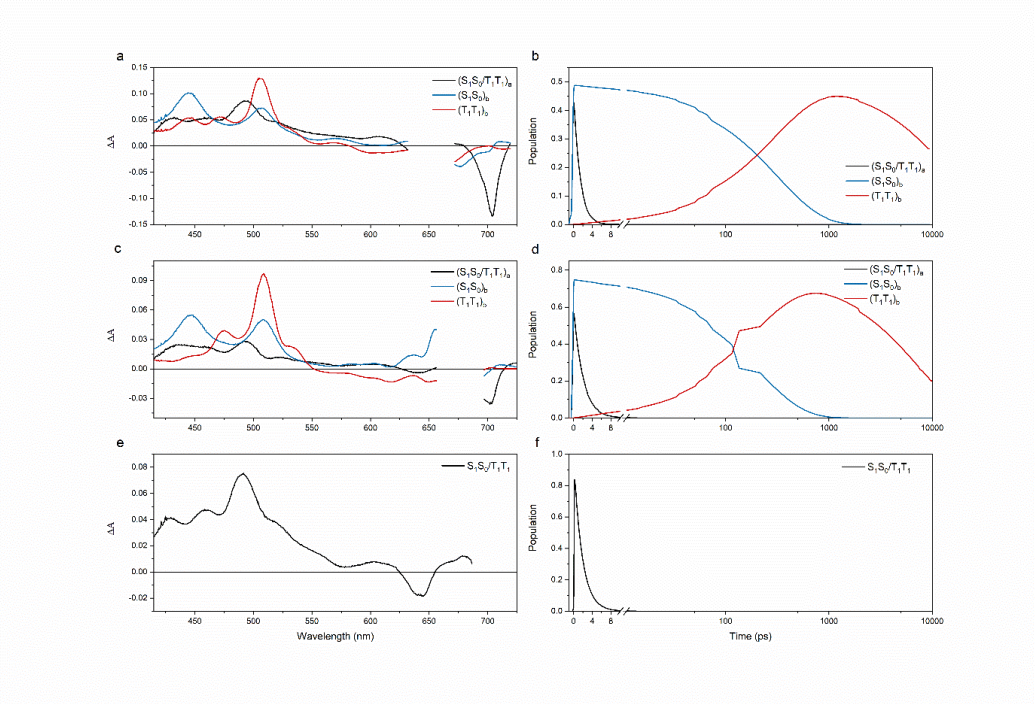

Figure S11.11. SAS and corresponding population dynamics of **PD3** with an excitation wavelength of 651 nm (a,b), 675 nm (c,d), and 707 nm (e,f) for the data in Figure S11.10 using the model in Figure 11.12 for excitation wavelength 651 and 675 nm and the model in Figure 11.13 for 707 nm.

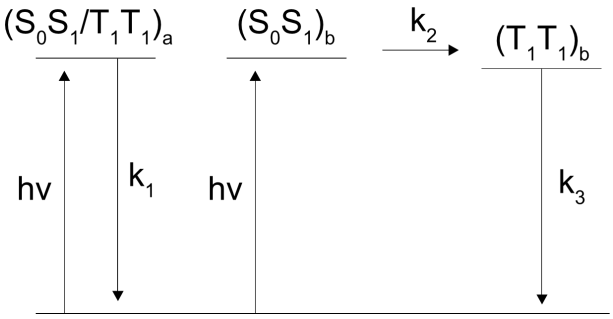

Figure S11.12. Kinetic model used to fit the transient absorption data at 100 K for **PD3** in Figure S11.10 with an excitation wavelength of 651 and 675 nm.

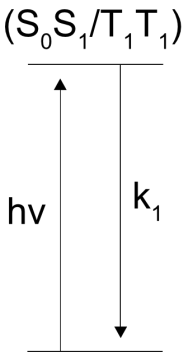

Figure S11.13. Kinetic model used to fit the transient absorption data at 100 K for **PD3** in Figure S11.10 with an excitation wavelength of 707 nm.

Table S11.4. Rate constants for **PD3** at 100 K in MTHF using the kinetic model in Figure S11.12 for excitation wavelengths 651 and 675 nm and Figure 11.13 for excitation wavelength 707 nm.

Excitation wavelength (nm)	$1/k_1$ (ps)	$1/k_2$ (ps)	$1/k_3$ (ps)
651	1.4	319	15000
675	2.1	212	7430
707	1.8	-	-

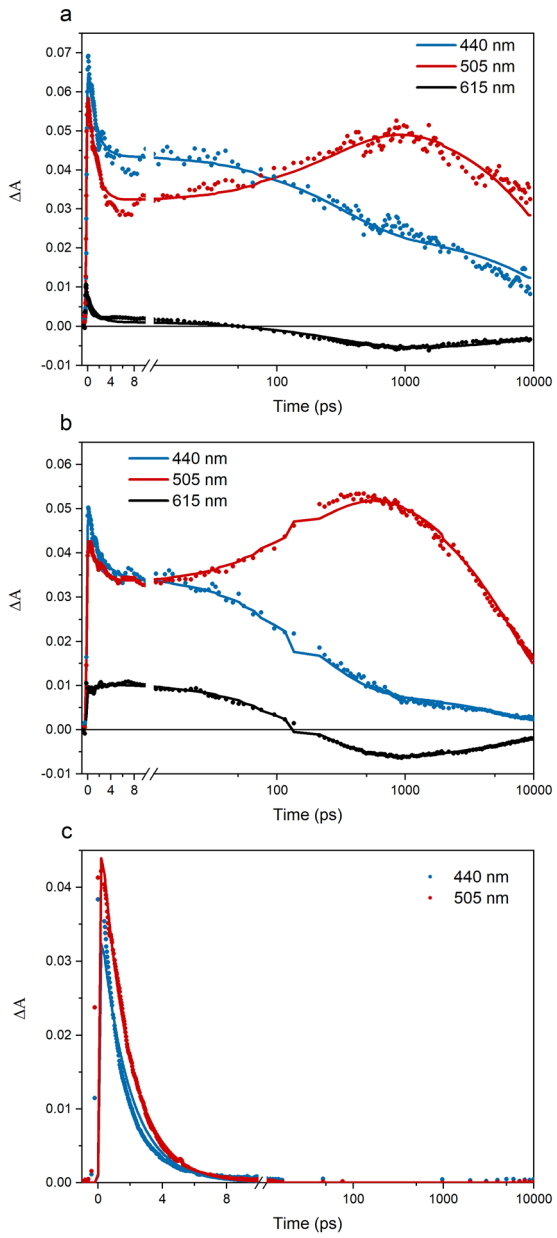

Figure 11.14. Kinetic traces of the raw data and fittings from the global analysis for a few select wavelengths for **PD3** with an excitation wavelength of (a) 651 nm, (b) 675 nm, and (c) 707 nm.

12. Temperature dependent fsTA

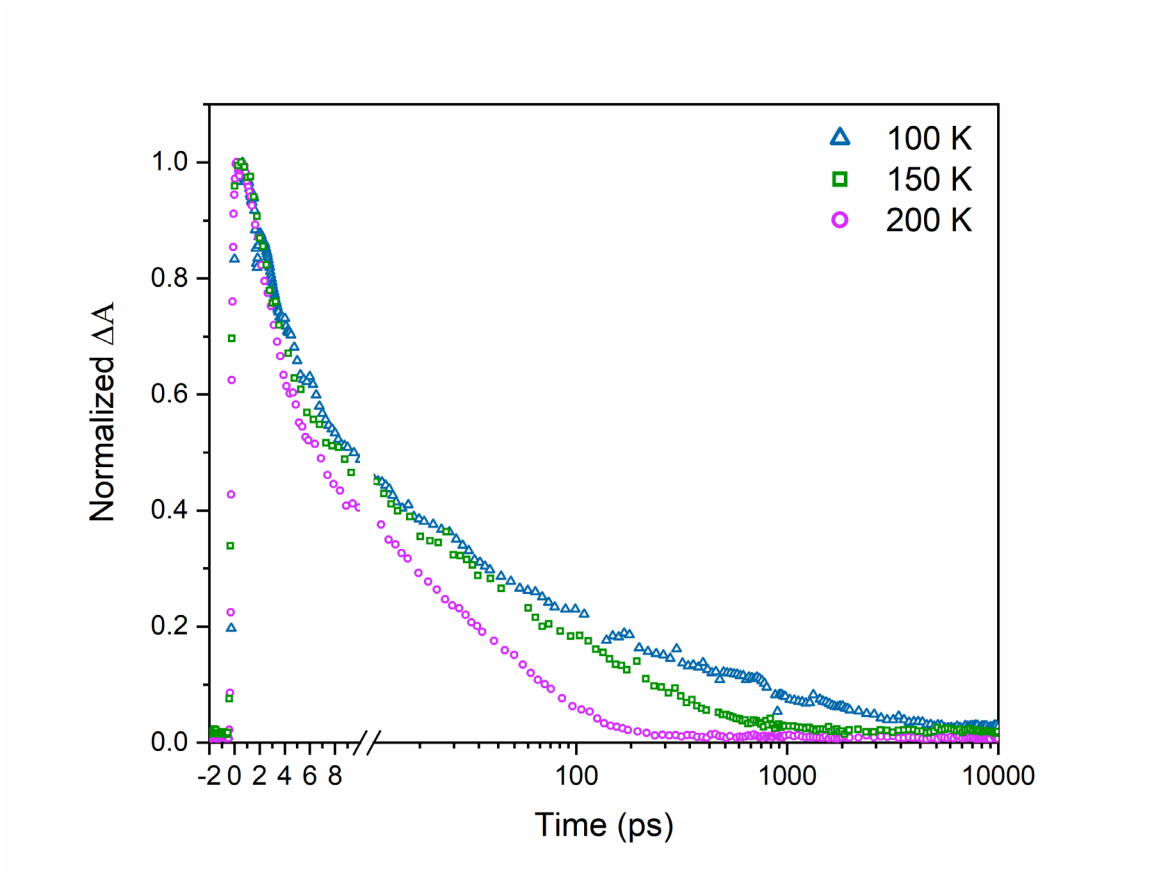

Figure S12.1. Single wavelength kinetics of the triplet-pair peak of **PD1** at 505 nm following excitation at 628 nm at 100, 150, and 200 K.

13. SF in polystyrene matrix

The polystyrene films were prepared by dissolving polystyrene pellets (average molecular weight = 250 000 g/mol, ACROS Organics) in toluene to 400 mg/ml. 1.2 ml of the polystyrene solution was transferred to 0.4 ml of ~100 µM **PD1** in toluene. The mixture was thoroughly mixed for 3h and then drop-casted on a glass substrate. The films were dried overnight. Similar procedure was performed for **PD2** and **PD3**.

Figure S13.1 presents the absorption spectra of **PD1–3** in toluene and in polystyrene. The absorption spectra in polystyrene are slightly red shifted for all three dimers and weak light scattering caused by the polymer film is observed.

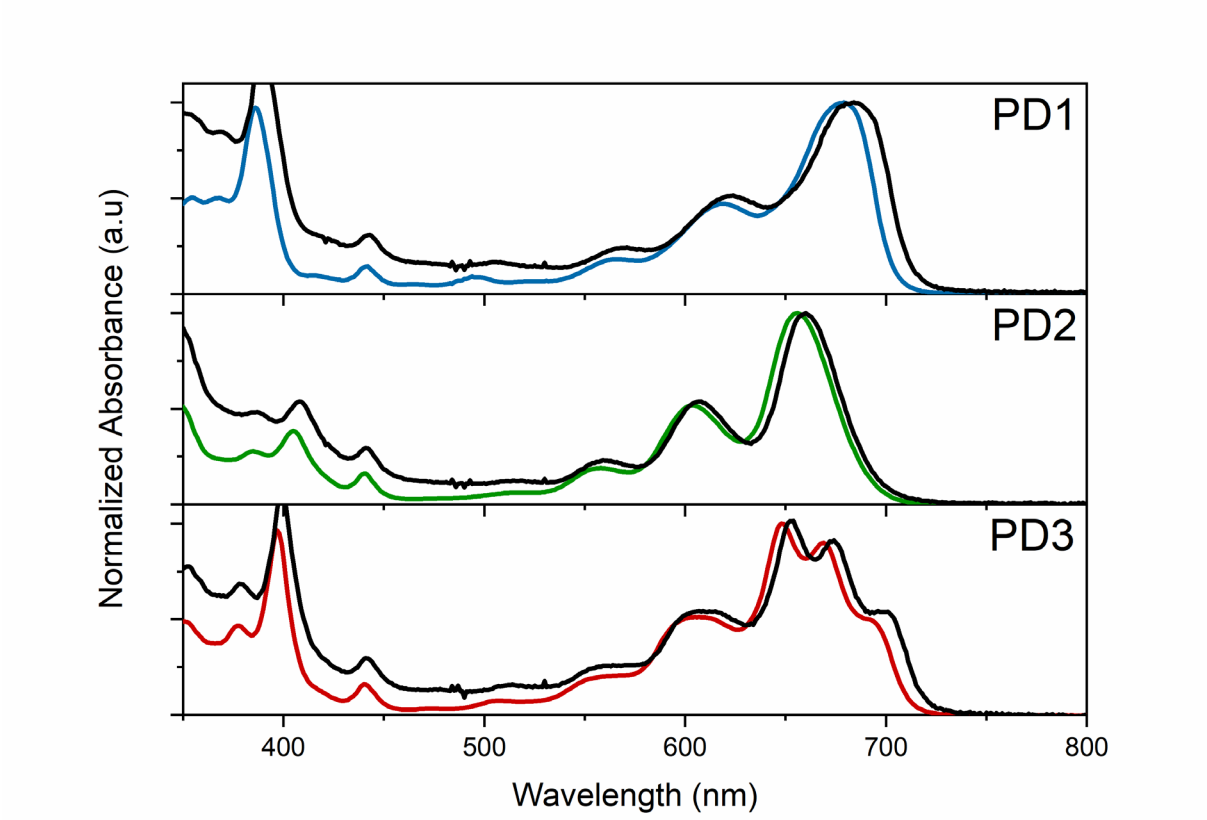

Figure S13.1. Comparison of the absorption spectra of **PD1** (blue), **PD2** (green), **PD3** (red) in toluene with the respective dimers in polystyrene (black).

13.1. fsTA of polystyrene films.

Figure S13.2 presents the transient absorption spectra of the dimers in polystyrene and Table S13.1 presents the obtained lifetimes from the kinetic analysis of triplet formation and decay using the equation below. The slight discrepancy between the time constants obtained from global analysis (Table S6.1) and tail-fitting for the toluene samples (Table S13.1) is ascribed to the presence of overlapping signals at the selected wavelengths, which reduces the accuracy of the tail-fitting procedure.

$$y = \sum A_i e^{-x/t_i}$$

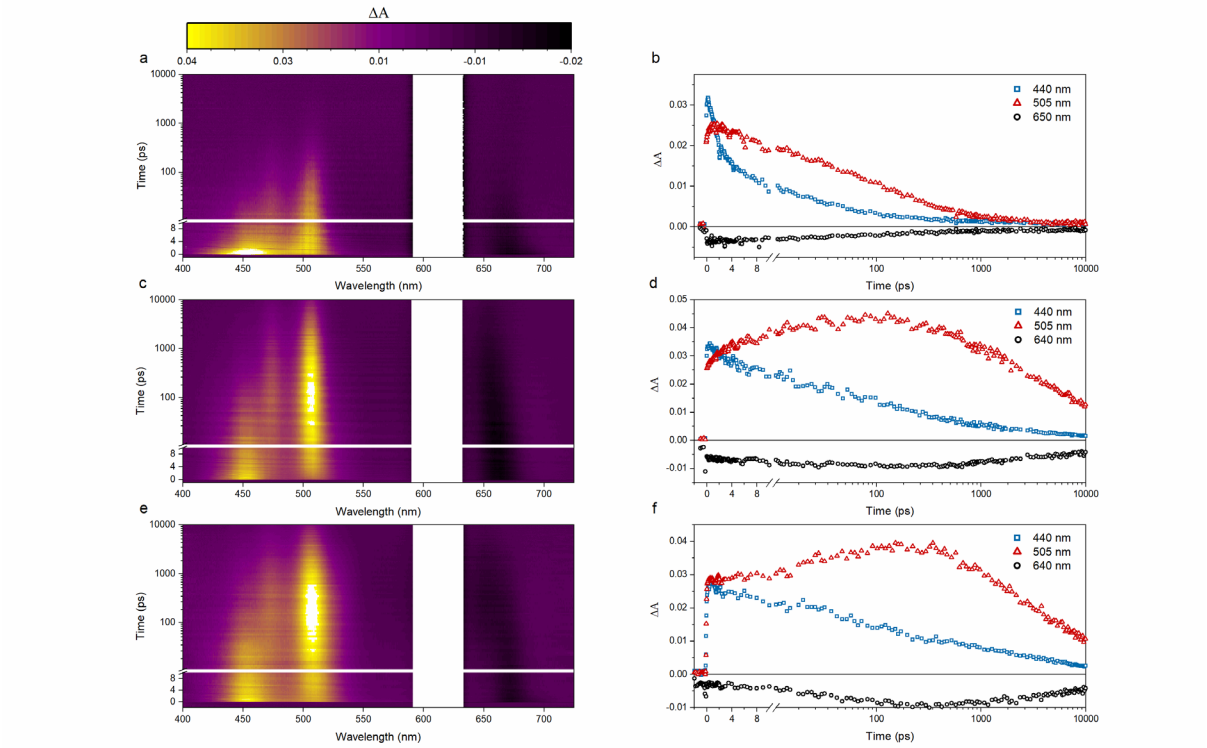

Figure S13.2. Room temperature transient absorption spectra and corresponding single wavelength kinetics of dimers **PD1** (a,b), **PD2** (c,d), and **PD3** (e,f). The measurements were performed in polystyrene matrices with a pump pulse at 612 nm. The pump scatter near the excitation wavelength has been removed for clarity.

Table S13.1. fsTA time constants from tail-fits of **PD1**, **PD2** and **PD3** triplet-pair formation and decay at 505 nm in toluene and polystyrene with a pump pulse at 612 nm. The data was normalized prior to the tail-fitting analysis. The rise time of the triplet pair is under-resolved for **PD1** in both polystyrene and toluene. The final row shows the amplitude weighted average lifetime of the decays.

	PD1 toluene	**PD1** polystyrene	**PD2** toluene	**PD2** polystyrene	**PD3** toluene	**PD3** polystyrene
$A_{T1T1,\ rise}$			–0.56	–0.36	–0.56	–0.33
$A_{T1T1,\ decay}$	1.0	0.47, 0.25	1.30	0.40, 0.57	1.31	0.50, 0.54
$\tau_{T1T1,\ rise}$ (ps)	-	-	10.3	9.3	27.6	45.8
$\tau_{T1T1,\ decay}$ (ps)	13	90, 690	98	1450, 13500	177	1660, 13690
$\tau_{average}$ (ps)	13	298[a]	98	8610[b]	177	7960[c]

[a] Amplitude average of lifetimes $\tau_{T1T1,\ decay}$. [b] Amplitude average of lifetimes of $\tau_{T1T1,\ decay}$. [c] Amplitude average of lifetimes $\tau_{T1T1,\ decay}$.

References

1. D. Lehnherr, A. H. Murray, R. McDonald and R. R. Tykwinski, *Angewandte Chemie International Edition*, 2010, **49**, 6190-6194.
2. J. D. Tovar and T. M. Swager, *Journal of Organometallic Chemistry*, 2002, **653**, 215-222.
3. S. Luliński and J. Serwatowski, *The Journal of Organic Chemistry*, 2003, **68**, 5384-5387.
4. J. Zirzlmeier, D. Lehnherr, P. B. Coto, E. T. Chernick, R. Casillas, B. S. Basel, M. Thoss, R. R. Tykwinski and D. M. Guldi, *Proceedings of the National Academy of Sciences*, 2015, **112**, 5325-5330.
5. C. Ruckebusch, M. Sliwa, P. Pernot, A. De Juan and R. Tauler, *Journal of Photochemistry and Photobiology C: Photochemistry Reviews*, 2012, **13**, 1-27.
6. I. H. M. Van Stokkum, D. S. Larsen and R. Van Grondelle, *Biochimica et Biophysica Acta (BBA) - Bioenergetics*, 2004, **1657**, 82-104.
7. Gaussian 16, Revision C.01, M. J. Frisch, G. W. Trucks, H. B. Schlegel, G. E. Scuseria, M. A. Robb, J. R. Cheeseman, G. Scalmani, V. Barone, G. A. Petersson, H. Nakatsuji, X. Li, M. Caricato, A. V. Marenich, J. Bloino, B. G. Janesko, R. Gomperts, B. Mennucci, H. P. Hratchian, J. V. Ortiz, A. F. Izmaylov, J. L. Sonnenberg, D. Williams-Young, F. Ding, F. Lipparini, F. Egidi, J. Goings, B. Peng, A. Petrone, T. Henderson, D. Ranasinghe, V. G. Zakrzewski, J. Gao, N. Rega, G. Zheng, W. Liang, M. Hada, M. Ehara, K. Toyota, R. Fukuda, J. Hasegawa, M. Ishida, T. Nakajima, Y. Honda, O. Kitao, H. Nakai, T. Vreven, K. Throssell, J. A. Montgomery Jr., J. E. Peralta, F. Ogliaro, M. J. Bearpark, J. J. Heyd, E. N. Brothers, K. N. Kudin, V. N. Staroverov, T. A. Keith, R. Kobayashi, J. Normand, K. Raghavachari, A. P. Rendell, J. C. Burant, S. S. Iyengar, J. Tomasi, M. Cossi, J. M. Millam, M. Klene, C. Adamo, R. Cammi, J. W. Ochterski, R. L. Martin, K. Morokuma, O. Farkas, J. B. Foresman and D. J. Fox, Gaussian, Inc., Wallingford CT, 2016.
8. K. Lopata, R. Reslan, M. Kowalska, D. Neuhauser, N. Govind and K. Kowalski, *Journal of Chemical Theory and Computation*, 2011, **7**, 3686-3693.
9. S. N. Sanders, E. Kumarasamy, A. B. Pun, M. T. Trinh, B. Choi, J. Xia, E. J. Taffet, J. Z. Low, J. R. Miller, X. Roy, X. Y. Zhu, M. L. Steigerwald, M. Y. Sfeir and L. M. Campos, *Journal of the American Chemical Society*, 2015, **137**, 8965-8972.
10. M. T. Trinh, A. Pinkard, A. B. Pun, S. N. Sanders, E. Kumarasamy, M. Y. Sfeir, L. M. Campos, X. Roy and X. Y. Zhu, *Science Advances*, 2017, **3**, e1700241.
11. S. Khan and S. Mazumdar, *The Journal of Physical Chemistry C*, 2020, **124**, 1171-1177.
12. M. Gilbert and B. Albinsson, *Chemical Society Reviews*, 2015, **44**, 845-862.
13. R. Mondal, C. Tönshoff, D. Khon, D. C. Neckers and H. F. Bettinger, *Journal of the American Chemical Society*, 2009, **131**, 14281-14289.